THE ASTROPHYSICAL JOURNAL, 443:818–836, 1995 April 20

MAGNETOSTATIC STRUCTURES OF THE SOLAR CORONA. II. THE MAGNETIC TOPOLOGY OF QUIESCENT PROMINENCES

B. C. LOW AND J. R. HUNDHAUSEN[1]
High Altitude Observatory, National Center for Atmospheric Research,[2] P.O. Box 3000, Boulder, CO 80307
Received 1994 July 20; accepted 1994 October 25

ABSTRACT

This paper treats the magnetic properties of the quiescent prominence as a part of the larger coronal structure made up of the prominence, cavity, and helmet dome. A rigorous analysis of the mechanical support of a vertical prominence sheet suspended in equilibrium by magnetic fields in uniform gravity shows that the finite vertical extension of the prominence sheet has an important dynamic constraint. For the inverse topology with the prominence magnetic field pointing opposite to the field implied by the bipolar photospheric region below, this constraint requires the prominence sheet to be embedded in a horizontal, nearly force-free, magnetic flux rope which crucially supports a part of the prominence weight by current attraction from above. A similar analysis of the support problem is carried out for the prominence in the normal topology in which both prominence and photospheric magnetic fields point in the same sense.

Starting with the observation that most prominences are of the inverse topology, a recent model is extended to show that this topology implies that the prominence sits in a two-flux magnetic system, one flux connecting the bipolar magnetic sources in the photosphere below and the other forming a rope which embeds the prominence and runs above and parallel to the photospheric polarity-inversion line. This model physically relates several pieces of well-known but hitherto disjoint observations. The prominence flux rope manifests itself as the cavity in the corona and as the filament channel in the chromosphere. The chromospheric fibril patterns associated with prominences and filament channels can, for the first time, be modeled faithfully. Several physical implications on the origin of the prominence and questions deriving from the results are discussed.

Subject headings: MHD — Sun: corona — Sun: prominences

1. INTRODUCTION

In the first paper of this series (Hundhausen & Low 1994, hereafter Paper I), we pointed out that the solar coronal helmet, as a long-lived structure, is often observed in scattered-white light to have a three-part structure: the high-density dome, the low-density cavity at the helmet base, and the quiescent prominence inside the cavity (e.g., Sime & Streete 1993). The large-scale corona observed with a coronagraph or at times of total eclipse has a complexity which varies with the level of solar activity (Newkirk 1967). At activity minimum, the corona has a simple configuration interpretable in terms of a dominant dipolar magnetic field tilted relative to the solar rotation axis (Hundhausen 1977). This magnetic field is closed low in the corona and over the magnetic equator but open elsewhere, giving rise to an equatorial belt of coronal helmet-streamers sandwiched in between extensive coronal holes centered respectively at the two magnetic poles (Pneuman & Kopp 1971). Figure 1 is a sketch of this coronal configuration idealized to be axisymmetric about the axis of the dipolar magnetic field. At activity maximum, the dipolar component of the large-scale magnetic field changes sign over a period of 1–2 years (Howard 1972; Parker 1979). The corona is then highly structured, with several complex belts of helmet-streamers associated with a multipolar magnetic field. Despite this variation in the complexity of the corona as a whole, the three-part structure of a helmet appears to be common and basic (Saito & Hyder 1968; Saito & Tandberg-Hanssen 1973; Sturrock & Smith 1968).

Traditionally, the quiescent prominence has been studied by ignoring the cavity in which it is observed to be embedded, and the cavity as a substrcture of the helmet has not received much attention in terms of its physical significance (Tandberg-Hanssen 1974; Zirin 1988; Priest 1989; Amari 1990). In this paper we analyze the magnetic support of the quiescent prominence in the hydromagnetic approximation, and demonstrate an intimate relationship between the prominence and its cavity. Once this relationship is appreciated, it will become intuitively clear how the helmet dome would complete the three-part structure with its apparent mechanical stability.

We start in § 2 with the classical problem of the magnetic support of the prominence as a heavy object in the corona. We will combine an observational inference on prominence magnetic topology with a mathematical theorem to show that the distributed electric-current density in the large-scale corona is vital to the support of prominences. This important point has been overlooked in most previous theoretical models. Simple illustrative models are treated in § 3, making use of the mathematical development of Paper 1. In § 4 we summarize the results and conclude with a discussion of physical implications and outstanding questions.

2. THE MAGNETIC TOPOLOGIES OF PROMINENCES

This section consists of two parts. We first describe the prominence based on a variety of observations. Then we treat the relationship between magnetic topologies and weight support.

[1] Department of Mathematical and Computer Sciences, Colorado School of Mines, Golden, CO.
[2] The National Center for Atmospheric Research is sponsored by the National Science Foundation.

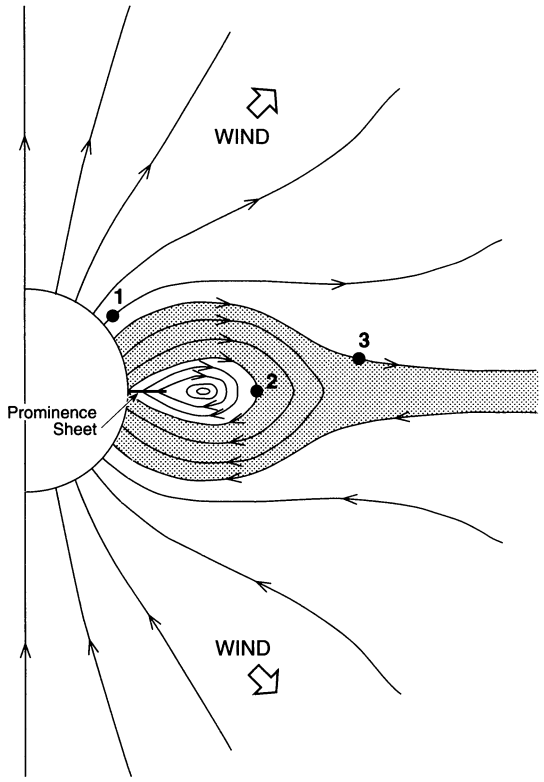

FIG. 1.—Sketch of the solar corona taken to be symmetric about both the axis and the equator of a large-scale dipolar magnetic field. As indicated by the arrowed lines of force, the corona is divided into an equatorial region of static closed-field region sandwiched between the high-latitude open-field regions where the expanding solar wind flows. The three-part structure of the coronal helmet-streamer is shown as the shaded high-density dome blending into the streamer containing the magnetic field reversal sheet; the low-density cavity characterized by a magnetic field closed entirely within the cavity; and the prominence idealized as an infinitesimally thin sheet encircling the Sun above the magnetic equator. The open magnetic field is poloidal, but an azimuthal field component is present in the magnetic fields which are either completely closed or anchored at the base, so that the arrowed lines for the latter are to be interpreted as lines of force projected onto the meridian plane. The three points labeled numerically are referred to in the text.

2.1. *Observations*

Quiescent prominences are cool and dense plasma condensations ($\sim 10^4$ K, $\sim 10^{11}$ H cm^{-3}) suspended by magnetic fields in the hot and tenuous solar corona ($\sim 10^6$ K, $\sim 10^8$ H cm^{-3}). These condensations persist from days to weeks, forming throughout the solar cycle. The quiescent prominences appear on the solar disk as a long, thin absorption feature in Hα located over a line of magnetic-polarity inversion on the photosphere. Observers refer to the prominence as the filament when it is seen as an absorption feature. When viewed at the solar limb in its own Hα emissions, the prominence shows a variety of shapes but is generally much more extended in height (10^{4-5} km) than it is thick (~ 5000 km). Eventually many of the quiescent prominences disappear abruptly, expelled through the corona into interplanetary space embedded within a coronal mass ejection (Illing & Hundhausen 1986; Hundhausen 1994; Kahler 1987; Low 1990; MacQueen 1980).

The magnetic field is central to the formation of prominences (Tandberg-Hanssen 1974; Anzer 1989). It provides support against gravity for the (electrically) highly conducting prominence. It also acts as a thermal shield for the cool prominence against the million degree coronal environment. Unfortunately, the magnetic field in the corona cannot be directly measured with any kind of useful spatial resolution. It is possible to measure only the magnetic fields in the photosphere and in the dense prominence. Nevertheless, these limited measurements have revealed two distinct basic configurations for the coronal field around a prominence, the so-called normal and inverse configurations (Anzer 1989; Leroy 1989, and references therein). In the former, the photospheric polarity beneath the prominence implies a magnetic field pointing in the same direction as the magnetic field threading across the prominence. In the latter, these two magnetic fields point in opposite directions. In both configurations, the magnetic field generally threads across the prominence at a shallow angle of about 20° to the long (horizontal) prominence axis. The strong axial component of the field gives rise to the often observed helical structures in erupting prominences (e.g., Tandberg-Hanssen 1974; House & Berger 1987; Vrsnad, Ruzdjak, & Rompolt 1991).

Observations have revealed that long quiescent prominences forming or persisting during the decay of a solar active region tend to lie in a cavity at the base of a well-formed coronal helmet, running above the polarity-inversion line of an extensive bipolar region on the photosphere. These prominences also tend to be located higher into the corona ($>30{,}000$ km above the photosphere) than the active variety associated with an active region, the latter tending to be shorter in length and often contorted in shape as a reflection of the complex active-region magnetic fields. Examples of the former are the so-called crown filaments forming in the high latitudes at the edge of an extensive polar region of unipolar open magnetic fields, early or late in a solar cycle. An observational result to which we will later give physical significance is that most prominences, and, in particular, those associated with the helmet-streamers have the inverse configuration (Leroy, Bommier & Sahal-Brechot 1984; Leroy 1989). Examples of the normal configuration have been found only for some of the lower-lying prominences (Athay et al. 1983; Leroy 1989).

The highly inhomogeneous chromosphere observed in Hα appears as a chaotic sea of fiber-like structures reasonably interpreted to be delineating tubes of magnetic flux emanating from the photosphere (Foukal 1971; Zirin 1988). Typically these structures show sharp contrast as absorption features against the chaotic background with lifetimes of the order of minutes to hours. The structures are short and tend to be vertically oriented over the quiet regions of the photosphere where the average magnetic intensity is 1–10 G. Over an active region where fresh magnetic flux has emerged through the photosphere with magnetic intensities ranging from 50 to 2000 G, the chromospheric fibrous structures tend to be horizontal, thin ($\sim 10^3$ km), and elongated ($\sim 10^{4-5}$ km). These active-region structures have been studied extensively. Although there are observationally meaningful distinctions between the rich variety of chromospheric structures, let us simplify for the purpose of this paper by calling all of them chromospheric fibrils. The reader is referred to Foukal (1971) for an excellent observational review.

Of particular interest to us in this paper is the well-established observation that over an active region the fibrils in the neighborhood of a filament take on a characteristic organized pattern as sketched in Figure 2 (Foukal 1971; McIntosh 1972; Martin, Bilimoria, & Tracadas 1993). As one approaches the dark filament from either side, the fibrils are

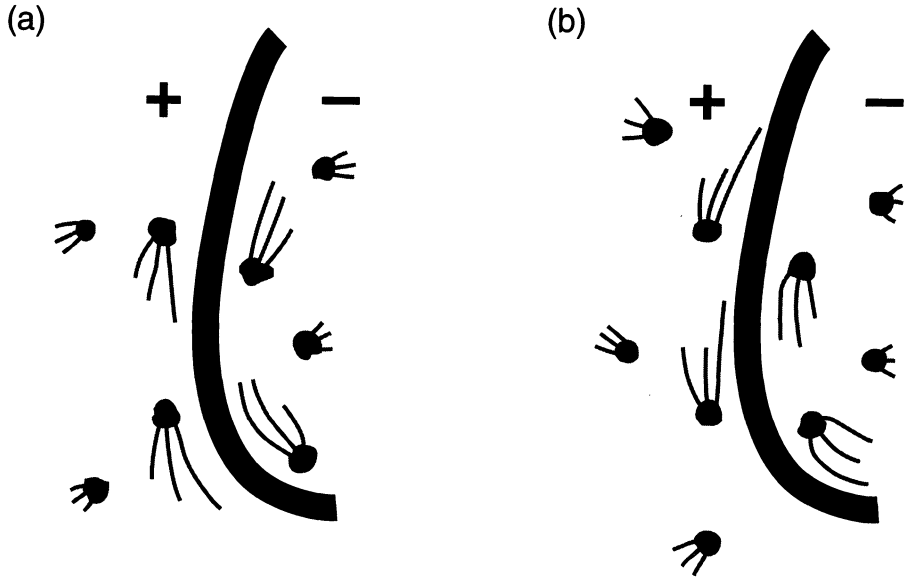

FIG. 2.—Sketch of the observed characteristic fibril pattern in the chromosphere in the neighborhood of an active-region filament. In the two configurations shown, described by Martin et al. (1995) as sinistral (*a*) and dextral (*b*), the thick long structure represents the filament seen projected on the chromosphere marking the magnetic polarity inversion line. The magnetic polarities of the two regions on the two sides of the filament are as indicated. The thin lines represent fibrils, anchored at chromospheric structures represented as black "knots," seen in projection, showing long lines near the filament and shorter lines located away from the filament.

found to be longer, more aligned parallel to the filament, all turning in the same general sense to stream parallel to the filament. At either side of the filament, the fibrils are locally parallel to the filament. Away from the filament, the fibrils are oriented perpendicular to the general direction of the filament. From the observed signs of magnetic polarities on the two sides of the filament, two feature are significant and intriguing: (1) no fibrils near the inversion line arc over it, and, (2) away from the inversion line, the fibrils imply that the magnetic fields in the positive and negative magnetic regions point away from and toward the inversion line, respectively. These two features are contrary to the morphology of a potential-like magnetic field. As shown in Figure 2, there are two types of fibril patterns. Consider the fibrils on the side of the filament where the magnetic polarity is positive. To an observer facing the filament on that side, the fibrils streaming parallel to the filament may stream either to the right or to the left. Martin et al. call the pattern with the former property dextral and the other sinistral.

Conventional techniques of magnetic field measurement require the detection of line emission from the prominence located at the solar limb. Active-region filaments are generally too low lying and rapidly evolving for these techniques to be usefully employed. Hence there are no reliable direct measurements of the magnetic fields in active-region filaments. With inferences drawn from the fibril patterns around filaments and the aid of the measurements of the line-of-sight magnetic fields in the photosphere, a strong case can be made that most if not all active-region filaments are not compatible with the normal magnetic topology, whereas they are not inconsistent with the inverse magnetic topology (Foukal 1971; Martin et al. 1993). If this conclusion is accepted, we can expect those more quiescent prominences, which are associated with decaying active regions and known to have the inverse magnetic topology by direct field measurements, to also manifest similar fibril patterns in the chromosphere. The fibrils in the quieter part of the solar atmosphere are considerably less conspicuous, and it is uncertain at the present time whether the expected characteristic fibril patterns can be observationally established for the quiet-region prominences. This lack of information is due to a traditional preoccupation with the active region in the study of solar activity.

It is important to note that both quiescent and active-region prominences, if large enough to be observed on the disk in radio waves, show a region of depressed radio emissions attributed to a low-density cavity around the filament (Drago & Felli 1970; Straka, Papagiannis, & Kogut 1975; Kundu, Melozzi, & Shevgaonkar 1986). Like their quiescent counterparts, the active-region filaments are also a component of a three-part structure though on a smaller scale: the filament, the cavity, and the higher-density low corona characteristic of active regions. For the purpose of this paper, we adopt the hypothesis that the quiescent and active-region filaments involve basically the same magnetic structure but may differ in magnetic intensity, geometric complexity, length scales of structure, and timescales of evolution. The archetypes of the long, stable, polar-crown filament and the short, contorted, rapidly evolving active-region filament are the two extremes of a spectrum of filament types all having the same basic magnetic structure. Our hypothesis serves as the starting point for our theoretical considerations in this paper. We should bear in mind that the observational basis of that hypothesis while persuastive is not without uncertainty. Magnetic vector field measurement for prominences at the solar limb is a complicated and difficult process beset with problems of noise, spatial resolution and line-of-sight effects; interpretations of optically thick chromospheric structures are never simple. However, as we shall see, taking our hypothesis as the starting point, interesting physical questions can be posed which have quite interesting and sensible answers.

2.2. *The Problem of Mechanical Support*

The theoretical problem of the prominence support is an old one (Anzer 1989). In the rest of this section, we derive an important dynamical constraint. For the present, we take the traditional approach of ignoring the cavity, which often encases, and the high-density dome which overlies a lengthy (10^{5-6} km) quiescent prominence. The simplest model of prominence support is the one treating the prominence as a vertical thin sheet of plasma, infinitely long in a given horizontal direction. Variation in that direction is ignored to keep the model two-dimensional, and the prominence is taken to be cold so that the prominence sheet is infinitesimally thin, with a (discrete) surface mass density. The latter approximation is reasonable for the consideration of the global magnetic configuration since the prominence density scale (height ~ 200 km) is negligible compared to the characteristic length (10^5 km) of the large-scale coronal magnetic field.

The weight of the plasma sheet is supported by the Lorentz force in static equilibrium as a first approximation. The Lorentz force arises from the static interaction between (a discrete) sheet of electric current, flowing horizontally along the infinitesimally thin prominence, and the coronal magnetic field. Most previous applications of this model assume that the coronal magnetic field around the prominence is potential. Under this assumption, the Lorentz force acting on the prominence can also be described in terms of the interaction between the prominence discrete current and the currents in the photosphere contributing to the coronal potential field. Using the simple rule that a pair of parallel line currents of the same sign mutually attract and of the opposite signs mutually repel, the mechanics of prominence support becomes quite transparent (Jackson 1965).

There are two aspects to the mechanics of prominence support. The net Lorentz force on the prominence must be upward in order to balance the downward total weight of the prominence. There is also the more stringent requirement of the detailed balance of the Lorentz force by the gravitational force on every piece of the prominence sheet as a spatially distributed object. This requires the Lorentz force to be upward everywhere on the prominence sheet. This condition is not obtainable for the inverse configuration, which is the principal result of this section. Of course, satisfying detailed force balance would imply net force balance, but it is instructive at this point in our presentation to separate these two aspects of force balance.

2.2.1. *Line Currents*

Let us first examine the support of the total prominence weight and then go into the detailed balance of forces. Consider the simplest model in which the spatial extent of the prominence is ignored by treating it as a line mass of density m per unit length suspended horizontally in a potential magnetic field by the Lorentz force due to a current flowing along the line mass.

Take the plane $z = 0$ to be the photosphere and the line mass to point in the x-direction, in standard Cartesian coordinates. Denote the current in the line mass by $I_{\rm prom}$. Let the corona be a perfect electrical conductor filled with a bipolar magnetic field anchored rigidly at the photosphere. For simplicity, take the prominence to have condensed at some height $z = z_2 > 0$ on the z-axis in the corona with no motion in the dense photosphere. Suppose the corona has a bipolar field due to a virtual current $I_{\rm photo}$ located at $z = z_1 < 0$ prior to the formation of the prominence. Then the induction of the current $I_{\rm prom}$ during the formation of the prominence must take place with the simultaneous appearance in $z < 0$ of its image with respect to the plane $z = 0$, so that the normal magnetic flux distribution given by $I_{\rm photo}$ is unchanged. The magnetic field in $z > 0$ after the prominence has formed is then derived from the magnetic stream function

$$A_{\rm line} = \frac{I_{\rm photo}}{c} \log \left[y^2 + (z - z_1)^2\right] + \frac{I_{\rm prom}}{c} \log \left[\frac{y^2 + (z - z_2)^2}{y^2 + (z + z_2)^2}\right], \quad (1)$$

where c is the speed of light. The magnetic feld is given by

$$\boldsymbol{B} = \nabla A_{\rm line} \times \hat{\boldsymbol{x}} . \quad (2)$$

The weight of the prominence per unit length is given by

$$mg = \frac{2}{c^2}\left[\frac{I_{\rm prom}^2}{2z_2} - \frac{I_{\rm prom} I_{\rm photo}}{(z_2 - z_1)}\right], \quad (3)$$

which determines the mass m per unit length in terms of g the gravitational acceleration and the current in the prominence and the photosphere.

For the line-current model, the two basic magnetic topologies of the quiescent prominence correspond to whether $I_{\rm prom}$ and $I_{\rm photo}$ are of the same sign or opposite signs, as illustrated in Figure 3. Later when we resolve the prominence into a spatially extended structure, we will be able to relate the difference between these two magnetic topologies to the sign of the magnetic field threading the prominence in the two cases. The example in Figure 3*a* corresponds to $z_1 = -1$, $z_2 = 0.75$, $I_{\rm prom}/I_{\rm photo} = -0.29$, in some arbitrary units. (Arbitrary units will be used in the models throughout this paper for convenience, since our interest is on the topological rather than the quantitative aspects of solar magnetic fields.) In Figure 3*a* the two line currents $I_{\rm prom}$ and $I_{\rm photo}$ are of opposite signs so that both terms on the right side of equation (3) are positive; note that $z_2 - z_1 > 0$ by definition. This is the normal configuration, in which the Lorentz force is always upward since the prominence is electrically repelled by *both* line currents in the photosphere. The other case shown in Figure 3*b*, with $z_1 = -1$, $z_2 = 0.2$, $I_{\rm prom}/I_{\rm photo} = 0.4$, is an example of the inverse configuration with $I_{\rm prom}$ and $I_{\rm photo}$ of the same sign. As equation (3) shows, the model is physical only for a sufficiently strong prominence current so that its repulsion by its image dominates over its attraction by the photospheric current $I_{\rm photo}$. This is the case in Figure 3*b*. The compression of the magnetic flux between the line prominence and the photosphere $z = 0$ is quite evident, giving rise to a net upward Lorentz force on the prominence. The example with $z_1 = -1$, $z_2 = 0.75$, $I_{\rm prom}/I_{\rm photo} = 0.4$ in Figure 3*c* is instructive. The Lorentz force on the line current is downward despite the similarity of the magnetic topology with that in Figure 3*b*. This example is physically not admissible.

The line-current model captures the essence of global support in the two basic magnetic topologies but says nothing about the internal structure of the prominence to which we now turn our attention.

2.2.2. *Sheet Currents*

Suppose the line current $I_{\rm prom}$ and its image in $z < 0$ are replaced with a discrete current flowing in the x-direction in the form of a vertical sheet intersecting the z-axis in the interval

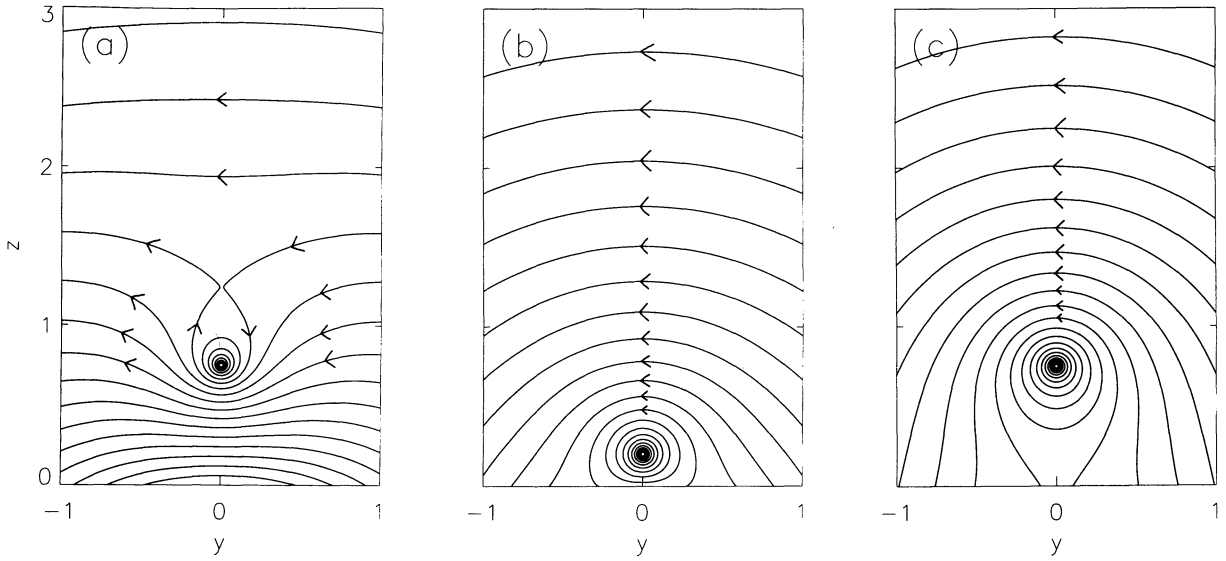

FIG. 3.—The normal and inverse magnetic configurations for prominences represented by line masses above the photosphere taken at $z = 0$. (*a*) A normal configuration around a line prominence with a current flowing opposite to the intrinsic photospheric current. (*b*) A inverse configuration around a line prominence with a current flowing in the same direction as the intrinsic photospheric current, such that the Lorentz force on the prominence is upward. (*c*) A inverse configuration similar to the one in (*b*) except that the Lorentz force on the prominence is downward. In all three cases, the photospheric current (not shown) is composed of the image current of the prominence and an intrinsic line current to account for the background bipolar magnetic field in $z > 0$. In this and other figures elsewhere, arrowed lines indicate magnetic lines of force.

$0 < a < z < b$, a and b being constants, combined with its image current sheet in $z < 0$. It is not convenient, in general, to represent the potential field due to a current sheet in terms of its stream function. For our purpose it suffices to consider a case in which the desired potential field has the explicit representation

$$B_y^{\text{prom}} - iB_z^{\text{prom}} = a_{\text{prom}}\{i[(\omega - ia)^{1/2} - (\omega - ib)^{1/2}]^2 - i[(\omega + ia)^{1/2} - (\omega + ib)^{1/2}]^2\}, \quad (4)$$

in terms of a free amplitude a_{prom} and the complex variable $\omega = y + iz$, with $i = (-1)^{1/2}$ (Coulson 1958). Figure 4 shows three examples of magnetic topologies generated by linear superpositions of the field given by equation (4) with the field due to the intrinsic photospheric line current I_{photo} given by the first term on the right side of equation (1). The examples in Figures 4*a* and 4*b* are clearly the extensions of the line-current models in Figures 3*b* and 3*a*, respectively, as distinguished by the sign of the current in the prominence sheet for a fixed sign of I_{photo}. With the prominence modeled as a sheet of finite vertical extent, we can now use the magnetic threading of the prominence to identify the topologies in Figures 4*a* and 4*b* to be of the inverse and normal type, respectively.

With the prominence sheet as a vertically resolved structure, the net Lorentz force is distributed along the sheet, where at each point it is to be balanced by the weight of the prominence's distributed (surface) mass. This is possible only if the Lorentz force is everywhere upward on the sheet, a requirement not to be taken for granted. The Lorentz force on the sheet is just the vertically directed, finite magnetic tension force associated with the abrupt turn or "kink" of the magnetic field line as it threads across the sheet. This is true for the models we consider, namely, those which are symmetric about the vertical sheet; see Wu & Low (1987) for a case where this symmetry is absent. The sign of the Lorentz force along the sheet is readily determined by an inspection of whether the magnetic kink implies an upward or downward tension force. In both examples in Figures 4*a* and 4*b*, the Lorentz force is upward on the lower part of the sheet but downward on the rest of the sheet. Force balance with gravity is therefore possible only in these lower parts. Both models are thus unphysical. Although these are particular solutions, these unphysical features are quite general and unavoidable for all inverse configurations and all normal configurations with closed magnetic lines of force. We prove this important point below.

Decompose the inverse magnetic field in Figure 4*a* in terms of the field due to the photospheric line current I_{photo} and the field given by equation (4), as shown, respectively, in Figures 5*a* and 5*b*. This decomposition is based on the principle of linear superposition for potential fields. Notice that the closed lines of force are nested around a point on the sheet where the horizontal field component vanishes. Crucially this point must lie within the sheet and not in the space around the sheet. Otherwise closed field lines will be found lying in their entirety in the potential field region of space. Ampere's law would then imply that currents must flow across the surfaces bounded by these closed field lines in the potential field region, and we have a contradiction. It is the lines of force circulating about the O-type magnetic neutral point located on the sheet that naturally give rise to a downward Lorentz force on the upper part of the sheet as indicated by the kink of the magnetic field at that location in Figure 5*b*. This conclusion is always true and easy to prove as follows for current systems superposed with their images about the plane $z = 0$.

The sheet and its image in Figure 5*b* can be further linearly decomposed into a set of current elements and their corresponding images, about $z = 0$, of equal but opposite current strengths. Consider the top of the sheet. The force it experiences is the sum of forces exerted by pairs of current elements, each pair made up of an element from the prominence sheet and its corresponding image in $z < 0$. For each pair, the attractive force exerted by the like-sign current element of the promi-

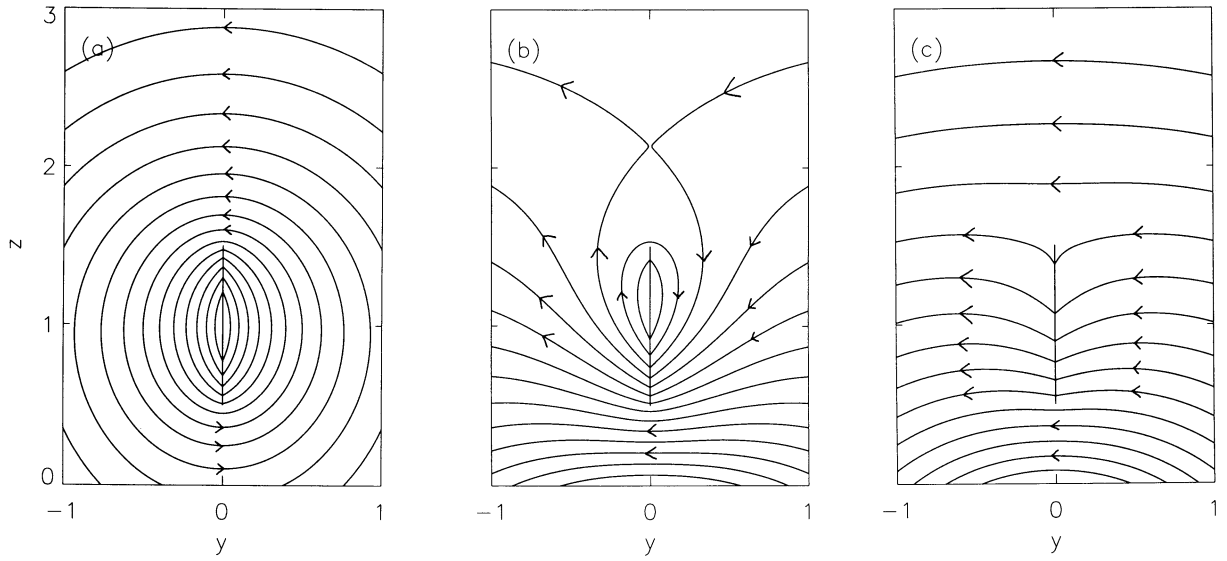

FIG. 4.—The inverse and normal magnetic configurations for prominences represented by vertical current sheets in $z > 0$. (*a*) A inverse configuration around a sheet prominence carrying currents flowing in the same direction as the intrinsic photospheric current. (*b*) A normal configuration around a sheet prominence carrying currents flowing opposite to the intrinsic photospheric current. (*c*) A normal configuration with a sufficiently strong intrinsic photospheric current such that no closed magnetic field is present in $z > 0$. In all three figures, the current sheet, shown as a vertical line, extends from $z = 0.5$ to 1.5 on the z-axis and has the same current distribution, and the photospheric current (not shown) is composed of the prominence image current sheet and an intrinsic line current giving the far-region bipolar field.

nence sheet is stronger than the repulsion force exerted by the image of that current element, located further away in $z < 0$. Hence, the net force on the top of the sheet is necessarily downward irrespective of the current distribution in the sheet. In other words, the self-pinching effect to collapse the sheet dominates over the repulsion force exerted by the image sheet, leading to the inevitability of the downward Lorentz force on the top of the sheet. This is a problem of internal structure which lies outside the approximation of line masses.

If this downward-acting Lorentz force is to be reversed in order to support the local mass at the top of the sheet, the current in the photosphere I_{photo} is the only means in the model to exert an additional, upward, Lorentz force. This requirement cannot be met in the inverse topology. In Figure 5*b*, the sign of the current in the sheet in $z > 0$ is positive by the right-hand rule, with the x-axis pointing out of the plane of the figure. In the inverse topology, the photospheric current has the same sign and it attracts the prominence current with an

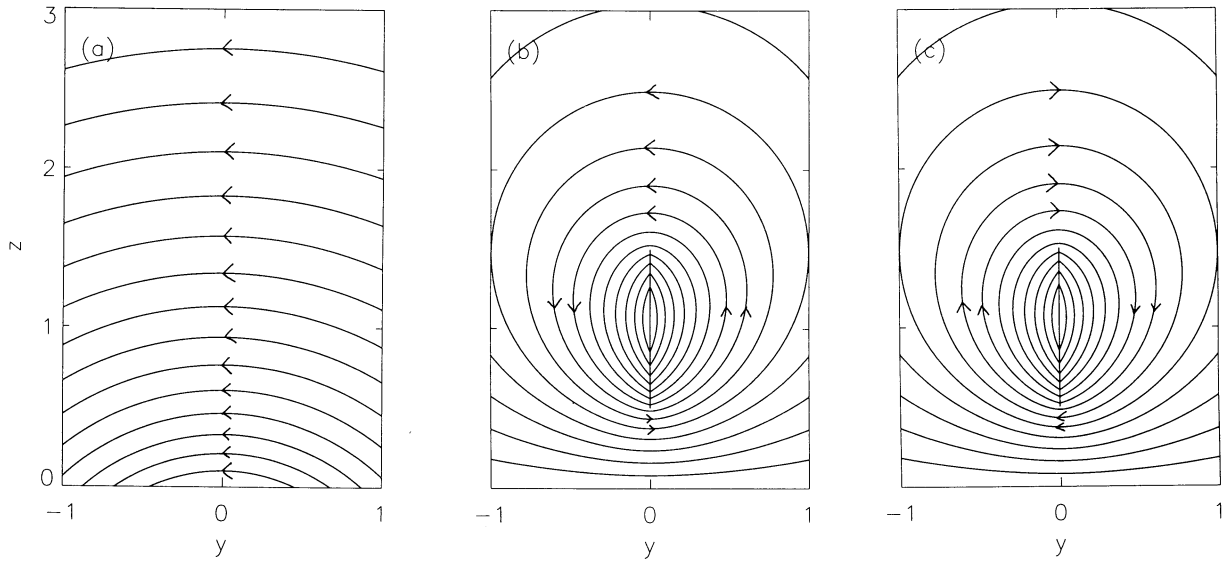

FIG. 5.—The potential magnetic fields whose superpositions produce the fields shown in Fig. 4: (*a*) The background bipolar magnetic field produced by an intrinsic line current in $z < 0$ on the z-axis. (*b*) The magnetic field contributed by the inverse-type prominence current sheet in Fig. 4*a* combined with its image current sheet in $z < 0$. (*c*) The magnetic field contributed by the normal prominence sheet in Fig. 4*b* combined with its image current sheet in $z < 0$. The current systems in (*b*) and (*c*) are the same but of opposite signs.

additional downward Lorentz force. The inverse magnetic configuration for the support of the prominence is therefore unphysical. By choosing a large enough net current in the prominence sheet for a given I_{photo}, it is possible to have the *net* Lorentz force on the prominence sheet acting upward, as is the case in Figure 4*a*, but the model always fails in the detailed force balance between the Lorentz and gravitational forces in the upper part of the prominence sheet. From the proof, it is clear that this is a completely general result not dependent on the specific distribution of the currents in Figure 4*a*.

The magnetic field in the normal configuration in Figure 4*b* is linearly decomposed into the field in Figure 5*a*, due to the photospheric line current, and that in Figure 5*c*, due to the prominence sheet and its image. The currents in Figures 5*b* and 5*c* are the same except for a change of sign. The above analysis of the Lorentz force again leads to the conclusion that in Figure 5*c*, the Lorentz force on the upper part of the prominence sheet is directed downward, due to the self-pinching tendency to collapse the sheet of current. The prominence sheet in this case has a negative current, opposite to that in Figure 5*b*. Consequently, the photospheric current I_{photo}, being positive, exerts a repulsive and, hence, an upward force on the prominence sheet. The possibility then exists for ensuring that the Lorentz force is everywhere upward on the prominence sheet by the superposition of a sufficiently large I_{photo} for a given prominence sheet current. In the case of the normal configuration in Figure 4*b*, the photospheric current I_{photo} is not strong enough to reverse the self-pinch Lorentz force at the top of the sheet. Hence, the net Lorentz force at the top of the sheet is downward as indicated by the kink of the magnetic lines of force threading this part of the sheet as shown. Figure 4*c* shows a case where the same prominence sheet is threaded by the field due to a sufficiently strong photospheric current I_{photo}, leading to an upward Lorentz force everywhere on the sheet. In this case, no closed magnetic fields occur in $z > 0$.

The presence of closed magnetic lines of force is topologically related to the unphysical downward direction of the Lorentz force somewhere on the sheet. Closed lines of force imply the presence of currents by Ampere's law. Hence, closed lines of force can only nest around an O-type neutral point necessarily located not in the potential field region but right on the prominence sheet. Then, with the sheet current being of a given sign, the Lorentz forces above and below the O-type neutral point are necessarily of the opposite signs. From this it follows that the normal configuration is physically admissible only if it contains no closed magnetic fields, such as in the case shown in Figure 4*c*.

It is instructive to consider the parametric change of magnetic topology for the normal configuration from that in Figure 4*b* to that in Figure 4*c* as the photospheric line current I_{photo} is increased from a sufficiently small value; the prominence sheet current and its image are held fixed. Topologically, it is clear that the presence of closed field lines around an O-type neutral point is associated with an X-type neutral point due to the bipolar nature of the "background" magnetic field contributed by I_{photo}. This latter neutral point can exist in the potential field region above the current sheet as shown for the case in Figure 4*b*. As I_{photo} increases in magnitude, its influence reduces and eventually reverses the net downward Lorentz force in the upper part of the prominence sheet. As the region with the unphysical downward Lorentz force shrinks in size, the O-type neutral point moves parametrically upward along the sheet while the X-type neutral point descends toward the sheet. At a critical value of I_{photo}, these two neutral points meet at the upper tip of the prominence sheet to form a cusp neutral point. At this critical point in parameteric change and beyond, as I_{photo} further increases, all points on the prominence sheet is supported by an upward Lorentz force.

We thus have the conclusion that the prominence sheet as a spatially extended object suspended in a bipolar potential magnetic field cannot be threaded by magnetic fields which are closed in the atmosphere. All inverse configurations and those normal configurations of the type shown in Figure 4*a* and 4*b* are ruled out. This conclusion is general in that it does not depend on the detailed distribution of the currents in the prominence sheet or the form of the photospheric current, whether the latter is a line current or a distributed current density in the photosphere. What is crucial for the proof of the conclusion are (1) the prominence sheet has currents of one sign, and (2) the photospheric currents generate a bipolar potential field in the atmosphere, the two basic features of the standard model treated in the literature.

Up to the time of the review by Anzer (1989), standard models of the normal configuration with no closed field lines have been reported; whereas, many attempts at producing the inverse configuration have been unsuccessful. Once the above fundamental reason for this general failure is recognized, we have the obvious conclusion that the inverse configuration requires the presence of volumetric currents in the surrounding corona to exert additional forces for prominence support. The assumption that the magnetic field around the prominence sheet is potential must be given up. In this connection, the potential model of Demoulin & Forbes (1992) is interesting. They recognized the basic difficulty of support for the top of the inverse-type prominence sheet resulting from the self-pinching effect, although no demonstration of the generality of that difficulty was given. To remove that difficulty within their potential model, they introduced an external line current of the same sign directly above the prominence sheet to provide an additional upward Lorentz force on the sheet. This model is a step in the right direction, but its treatment of the support difficulty is not quite satisfactory because the external line current cannot be given an unambiguous interpretation. As we saw in this section, important physics may be approximated out of the model by the use of line currents. The needed additional upward Lorentz force on the inverse-type prominence sheet requires the presence of a spatially distributed electric current around the prominence. In the next section, we show that in this case, the simplest theoretical construction leads naturally to the embedding of the prominence in a low-density magnetic flux rope.

3. THE NECESSITY OF THE PROMINENCE CAVITY

The corona is both tenuous and (electrically) highly conducting. It can sustain a high electric current but cannot support any significant Lorentz force. Therefore, the presence of force-free magnetic fields around the prominence is the simplest way of introducing currents into the corona to produce a significant Lorentz force on the prominence without exerting a comparable force on the corona. Amari & Aly (1990) gave an example of the normal-type prominence sheet embedded in a force-free magnetic field. Earlier attempts to produce an inverse-type prominence sheet in a force-free magnetic field were successful only as a spatially local solution, leaving open the question of its proper match to the global field (e.g., Ridgway, Amari, & Priest 1991a, b; Cartedge & Hood 1993).

This technical problem of matching solutions was solved in the first successful global model for the inverse configuration, in which the prominence sheet is suspended in a horizontal rope of twisted, force-free magnetic field (Low 1993; hereafter L93).

It is natural to identify this magnetic flux rope with the commonly observed cavity around the prominence. Physically we expect the flux rope to be a locally enhanced magnetic field. Its density is likely to be reduced in order to be in pressure equilibrium with the surrounding plasma, the helmet dome, which we suggest has a weaker magnetic field but higher plasma pressure and density. However, a force-free magnetic flux rope does not interact with the coronal plasma. The force-free field therefore lies in a plane-parallel hydrostatic atmosphere, and will show no plasma structures indicating its presence. To explicitly account for the prominence cavity as a density-deficit region due to the presence of the magnetic flux rope, cross-field electric current density must be introduced into the coronal plasma around the prominence. The amount of cross-field current in the corona is probably weak compared to the field-aligned current of the twisted flux rope.

To begin to discuss such a complex hydromagnetic situation, a quantitative model is needed, and, to that end, we provide one in the next section based on the mathematical theory in Paper 1. Using this model, we will show how a variety of prominence properties and observations do relate physically as a whole.

3.1. *The n = 2 Polytropic Model*

We are interested in a magnetized atmosphere described by the equations of magnetostatic equilibrium:

$$\frac{1}{4\pi}(\nabla \times \boldsymbol{B}) \times \boldsymbol{B} - \nabla p - [\rho + m(S)\delta(S)]g\hat{z} = 0\,, \tag{5}$$

$$\nabla \cdot \boldsymbol{B} = 0\,, \tag{6}$$

where we introduce the coronal pressure p and density ρ, and take the gravitational acceleration g to be uniform in space directed along $-\hat{z}$ in Cartesian coordinates. The gravitational force includes that of a surface mass distribution m, described by a Dirac delta function, over some surface S to be interpreted physically as the prominence sheet.

For a two-dimensional system invariant in the x-direction, we have the standard representation of the divergence-free magnetic field

$$\boldsymbol{B} = \left(Q, \frac{\partial A}{\partial z}, -\frac{\partial A}{\partial y}\right), \tag{7}$$

in terms of two functions Q and A, the latter being the stream function which is constant along a magnetic line of force. For the situation of interest, it was shown in Paper I that equation (5) can be decomposed into the two components:

$$\frac{\partial p(A, z)}{\partial z} + \rho g = 0\,, \tag{8}$$

$$\nabla^2 A + Q\frac{dQ}{dA} + 4\pi\frac{\partial p(A, z)}{\partial A} + \frac{4\pi}{c}J_{\text{prom}}(S) = 0\,, \tag{9}$$

describing, respectively, hydrostatic equilibrium along the magnetic field and the balance of forces across the magnetic field. In this situation, we have a vertical current sheet S of infinite length in the x-direction and intersecting the z-axis, representing the prominence in a model which is symmetric about the z-axis. A discrete current J_{prom} flows in the x-direction in the prominence sheet, generating a Lorentz force which supports the prominence surface-mass density m per unit horizontal length according to the equation:

$$mg = \frac{1}{c}J_{\text{prom}}B_y\,, \tag{10}$$

where B_y is evaluated on the current sheet S.

The general mathematical model is formidable. For our purpose in this section, we select a particular model from the general class associated with a polytropic atmosphere given in Paper I. We omit the details of mathematical construction, which can be found in Paper I. For a self-contained presentation, we give a description of the mathematical solution of interest to us here and mention its essential physical properties. After having acquainted ourselves with the solution, we then resume our discussion of prominence modeling.

Consider a magnetized atmosphere located above the photosphere taken to be the plane $z = z_0$, a constant, such that one of the magnetic flux surfaces lies on the circle $r = [y^2 + z^2]^{1/2} = r_0$ of radius r_0 in the y-z plane and intersecting the line $z = z_0$, assuming $-r_0 < z_0 < r_0$. Call this flux surface $\partial\sigma$. Take the currents in this atmosphere to be located within $\partial\sigma$ so that its external region is a plane-parallel hydrostatic atmosphere embedding a potential magnetic field. Take the discrete current J_{prom} of the prominence sheet to be given, and prescribe

$$Q = \lambda A^{1/2}\,, \qquad \text{inside } \partial\sigma\,,$$
$$= 0\,, \qquad \text{outside } \partial\sigma\,, \tag{11}$$

$$p = \frac{a_0 + a_1 A}{(z + r_0)^2}\,, \qquad \text{inside } \partial\sigma\,,$$
$$= \frac{a_0}{(z + r_0)^2}\,, \qquad \text{outside } \partial\sigma\,, \tag{12}$$

$$\rho = \frac{2(a_0 + a_1 A)}{g(z + r_0)^3}\,, \qquad \text{inside } \partial\sigma\,,$$
$$= \frac{2a_0}{g(z + r_0)^3}\,, \qquad \text{outside } \partial\sigma\,, \tag{13}$$

where λ, a_0, and a_1 are constants. In this prescription we take with no loss of generality $A = 0$ on $\partial\sigma$ since the stream function is ill-defined up to a constant corresponding to the free gauge of the magnetic vector potential; see equation (7). Equations (11)–(13) are defined with the free constant of A fixed in this manner. The governing equations (8) and (9) are now well defined in the two regions inside and outside $\partial\sigma$, and the task is to match solutions for these two complementary regions across $\partial\sigma$ to obtain a global solution in $z > z_0$.

Note that the plasma is governed by a polytropic equation of state in the following sense (Paper I). Along a magnetic line of force, A has a constant value and the pressure $p \propto \rho^{1+1/n}$ with the polytropic index $n = 2$. Moreover, the hydrostatic equation (8) is automatically satisfied. The problem then reduces to solving equation (9) for A as the unknown for the two complementary regions to be matched across $\partial\sigma$. Outside $\partial\sigma$, we have a potential stream function satisfying

$$\nabla^2 A = 0\,, \tag{14}$$

and inside $\partial\sigma$, we have a nonpotential stream function satisfying

$$\nabla^2 A + \frac{1}{2}\lambda^2 + \frac{4\pi a_1}{(z + r_0)^2} + \frac{4\pi}{c}J_{\text{prom}}(S) = 0\,, \tag{15}$$

which effectively is Ampere's law giving the x-component of $\nabla \times \boldsymbol{B}$ in terms of contributions from the field-aligned current, the pressure-induced cross-field current, and the prominence sheet current.

The matching conditions at $\partial\sigma$ are that $A = 0$ by definition, and to ensure this plasma boundary is in force equilibrium, that the total pressure is continuous. The first condition and equations (11) and (12) imply that at $\partial\sigma$, the plasma pressure is continuous and $B_x = Q = 0$. It then follows from the second condition that A has continuous derivatives at the boundary. Subject to these conditions at $\partial\sigma$, a family of solutions can be generated by a linear superposition of four independent stream functions

$$A = A_{\rm shear} + A_{\rm prom} + A_{\rm corona} + A_{\rm pot}\,, \tag{16}$$

to be defined below.

The first term $A_{\rm shear}$ is taken from L93, being the contribution of the field-aligned current density proportional to the constant λ^2:

$$\begin{aligned} A_{\rm shear} &= \frac{\lambda^2}{8}(r_0^2 - r^2)\,, && \text{inside } \partial\sigma\,, \\ &= -\frac{\lambda^2}{8} r_0^2 \log\left(\frac{r^2}{r_0^2}\right), && \text{outside } \partial\sigma\,. \end{aligned} \tag{17}$$

The second term $A_{\rm prom}$ is the contribution of the prominence discrete current $J_{\rm prom}$. For our purpose, we take $A_{\rm prom}$ to be the stream function of the magnetic field

$$B_y^{\rm prom} - iB_z^{\rm prom} = a_{\rm prom}\left\{[(\omega + ia)^{1/2} - (\omega + ib)^{1/2}]^2 - \frac{r_0^2}{\omega^3}[(a\omega + ir_0^2)^{1/2} - (b\omega + ir_0^2)^{1/2}]^2 - i\frac{(a-b)^2}{4\omega}\right\}, \tag{18}$$

written in terms of the complex variable $\omega = y + iz$ and the constant amplitude $a_{\rm prom}$ (L93). This magnetic field is potential in the entire y-z plane except at two current sheets located on $y = 0$, $0 > -a > z > -b > -r_0$, and $y = 0$, $-r_0^2/b > z > -r_0^2/a$. These two current sheets are images with respect to the circle $r = r_0$ on which $\partial\sigma$ lies. Hence, one of its lines of force is coincident with $\partial\sigma$. Only the current sheet in the upper interval lies in the physical domain $z > z_0$, assuming $-b > z_0 > -r_0$, which we identify with the prominence sheet. The component $B_z^{\rm prom}$ is discontinuous across this current sheet, and we have by Ampere's law

$$J_{\rm prom} = \frac{c}{2\pi}\langle B_z^{\rm prom}\rangle_s\,, \tag{19}$$

where the angular bracket denotes the jump of a quantity across the sheet S. In effect we have prescribed $\boldsymbol{B}^{\rm prom}$ and obtained in a self-consistent manner the discrete current $J_{\rm prom}$ which generates it. In constructing $A_{\rm prom}$ from $\boldsymbol{B}^{\rm prom}$, we have a constant of integration which, with no loss of generality, is chosen so that $A_{\rm prom} = 0$ on $\partial\sigma$.

The third term $A_{\rm corona}$ has an amplitude proportional to a_1 and is the contribution of the pressure-induced cross-field current

$$\begin{aligned} A_{\rm corona} &= 4\pi a_1\left[\log\left(-\frac{\zeta}{\zeta_0}\right) + \frac{\zeta + \zeta_0}{\zeta_0}\right], && \text{inside } \partial\sigma\,, \\ &= 0\,, && \text{outside } \partial\sigma\,, \end{aligned} \tag{20}$$

given in terms of quantities to be defined below. We introduce the conformal mapping $\xi + i\zeta = 1/[y + i(z + r_0)]$:

$$\xi = \frac{y}{y^2 + (z + r_0)^2}\,, \qquad \zeta = -\frac{z + r_0}{y^2 + (z + r_0)^2}\,. \tag{21}$$

This mapping takes lines of constant ξ and ζ into two orthogonal families of circles in the y-z plane, which are all tangent at the point $y = 0$, $z = -r_0$ to the lines $y = 0$ and $z = -r_0$, respectively. The circular boundary $\partial\sigma$ then lines on $\zeta(y, z) = -\zeta_0$ where $\zeta_0 = 1/2r_0$, which is the circle $r = r_0$ centered at the origin. Note that by definition, $A_{\rm corona} = 0$ on $\partial\sigma$ and is identically zero outside this boundary.

The last term $A_{\rm pot}$ is an arbitrary potential stream function subject to the following requirement. By virtue of their constructions, $A_{\rm shear}$, $A_{\rm prom}$, and $A_{\rm corona}$ each independently vanish on $\partial\sigma$. In order that the net stream function A given by equation (16) preserves $\partial\sigma$ as a magnetic flux surface, we require $A_{\rm pot}$ to be constant on $\partial\sigma$, and, with no loss of generality, we take that constant to be zero so that $A = 0$ on $\partial\sigma$. A rich variety of potential magnetic fields possessing this property can be generated by discrete (virtual) current sources forming image pairs with respect to the circle $\zeta = -\zeta_0$ but lying in $z < z_0$, outside the domain of physical interest. For our purpose in this subsection, we choose the potential field $A_{\rm pot} = A_{\rm dipole}$ where

$$A_{\rm dipole} = a_{\rm dipole}(\zeta + \zeta_0)\,, \tag{22}$$

describing the field due to the classical point dipole of amplitude $a_{\rm dipole}$ located at $y = 0, z = -r_0$.

The stream function A given globally by equation (16) has continuous first derivatives across $\partial\sigma$. Together with Q given by equation (11) for the different regions of the domain, the magnetic field is then fully specified. In terms of the stream function A, the equilibrium distributions of the coronal plasma density and pressure given by equations (12) and (13) are also specified. In terms of the magnetic field at the prominence sheet S and the discrete current $J_{\rm prom}$, the prominence surface-mass density m is defined by equation (10). The model construction is then complete. We now turn to the application of this model to the discussion of the properties of the inverse-type prominence.

It should be noted that despite the use of linear superposition in constructing the stream function A, the solution is nonlinear for $\lambda \neq 0$; see equation (11). A second point to note is that equation (11) defines a meaningful $B_x = Q$ only if A is positive. More will be said about this point later.

3.2. *Application to the Inverse-Type Prominence*

The model in § 3.1 contains the free amplitudes λ, $a_{\rm prom}$, a_1, and $a_{\rm dipole}$, respectively, of the four independent terms on the right-hand side of equation (16). We leave the interested reader to survey the rich variety of solutions which can be generated. For our purpose, we select several particular explicit solutions to make quite specific physical points about the inverse-type prominence.

3.2.1. *Prominence in a Force-free Magnetic Flux Rope*

Figure 6 shows a superposition to obtain a prominence model of the inverse magnetic topology, previously treated in L93. We set $a_1 = 0$ and $a_{\rm dipole} = 0$ to suppress the cross-field current density in the corona and remove the dipole potential

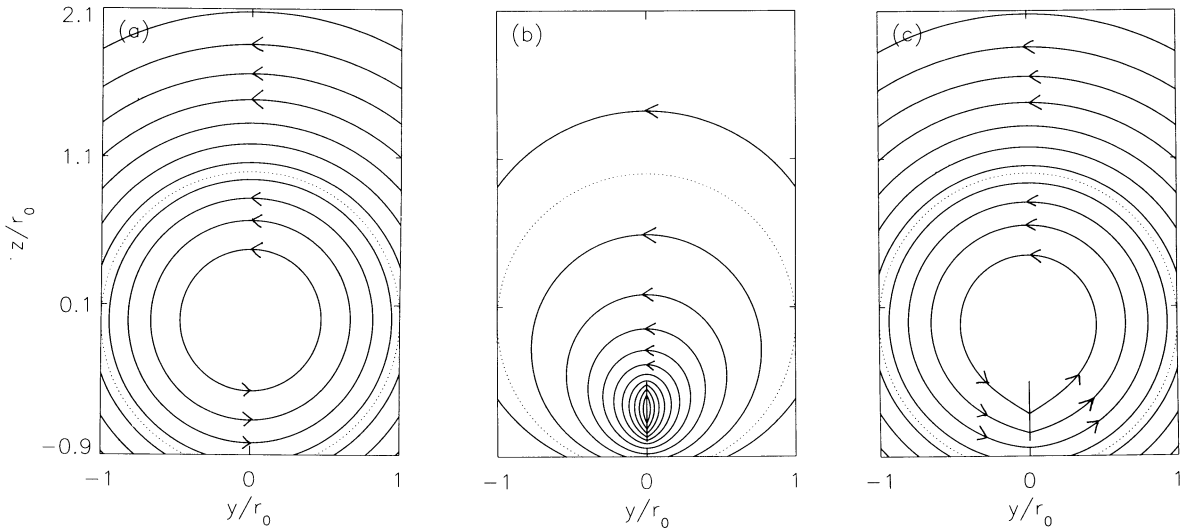

FIG. 6.—The linear superposition of magnetic fields to produce a inverse-type prominence sheet embedded in a flux rope of twisted magnetic fields. (*a*) The lines of force of the force-free magnetic field projected on the *y*-*z* plane generated by contours of constant $A_{\rm shear}$. These projected lines of force lie on circles centered at the origin. The magnetic field has a nonvanishing *x*-component in the region bounded by the dotted circle $r = r_0$ outside of which the field is potential, lying strictly in the *y*-*z* plane. (*b*) The potential magnetic field $\boldsymbol{B}_{\rm prom}$ due to a current sheet, represented by the vertical line, extending from $z = -0.4r_0$ to $z = -0.8r_0$ on the *z*-axis, and its sheet image with respect to the circle $r = r_0$. (*c*) The linearly superposed magnetic field representing the prominence as a sheet embedded in a magnetic flux rope above the photosphere taken at $z = -0.9r_0$, as described in the text.

field given by equation (22). The stream function $A_{\rm shear}$ generates the streamlines shown in Figure 6*a*, which are circles centered at the origin. The potential field $\boldsymbol{B}^{\rm prom}$ due to the prominence current sheet on the *z*-axis is shown in Figure 6*b* as streamlines of constant $A_{\rm prom}$. A superposition of these two stream functions, with $\lambda = 1.93$, $a_{\rm prom} = 1.0$, $a = 0.4$, $b = 0.8$, $z_0 = -0.9$, gives the stream function A shown in Figure 6*c* describing the magnetic field of the inverse-type prominence we set out to construct. In terms of A, equation (11) describes the distribution of the *x*-component of the magnetic field. Hence, Figure 6*c* is a display of the projection of the lines of force on the *y*-*z* plane.

The magnetic field depicted in Figure 6*c* has the following global topology which underlies all the inverse-type prominence models we will consider in this section. The dotted circles in Figure 6 represent the magnetic flux surface $\partial\sigma$ separating its current-filled interior from its potential exterior. In Figure 6*c*, the prominence is represented as a vertical current sheet suspended in a magnetic flux rope with $B_x \neq 0$ and fully detached from the base $z = z_0$. This flux rope is encased in an arcade of sheared, anchored bipolar magnetic field with $B_x \neq 0$. The arcade is bounded by $\partial\sigma$ outside of which an anchored, bipolar potential field is found, lying in the *y*-*z* plane with $B_x = 0$. In the arcade and the flux rope, the current density is parallel to the magnetic field except at the prominence sheet where a nonzero Lorentz force supports the prominence weight according to equation (10). Comparing the sense of the magnetic field threading the prominence sheet with that of the magnetic field implied by the bipolar magnetic sources at $z = z_0$, we see that this model has the inverse topology.

The significance of this model is that an O-type magnetic neutral point lies just above the prominence sheet, a feature not admissible in the standard models which take the field around the prominence to be potential. This O-type neutral point is admissible because of the presence of field-aligned current density in the region around the prominence sheet. As pointed out in L93, there is a net current of the surrounding force-free magnetic field flowing in the same sense in the *x*-direction as the discrete current in the prominence. The former is centered at the O-type neutral point and by its attraction *from above* helps to support the weight of the prominence. This attractive force from above, missing in the model in § 2, is crucial for the support of the upper part of the prominence sheet. Another way of viewing this support is that the upper part of the prominence sheet is supported in part by being suspended from the projected closed lines of force of the magnetic flux rope. This flux rope of helical fields is in turn held down in equilibrium by the overlying bipolar arches anchored to the photosphere. It also implies naturally a significant component of the prominence magnetic field along the long length of the prominence. Foukal (1971) and Leroy (1989) have pointed out that observations strongly support the presence of a strong axial magnetic field along the prominence which generally played no role in previous theoretical models.

Now, not any combination of $A_{\rm shear}$ and $A_{\rm prom}$ will yield a properly supported prominence. For a fixed $A_{\rm prom}$, the net current in the *x*-direction of the surrounding force-free magnetic field (generated by the contribution of $A_{\rm shear}$) must be of the same sign as $J_{\rm prom}$ and must exceed a threshold magnitude to ensure that the Lorentz force is everywhere acting upward on the prominence sheet. This translates into a requirement on λ so that B_y in equation (10) is positive on the sheet, or, explicitly,

$$-\frac{\lambda^2}{4} z + B_y^{\rm prom} > 0 , \tag{23}$$

along the sheet located at $-b < z < -a$. In this inequality $B_y^{\rm prom}$ is negative in the upper part of the interval for a given $a_{\rm prom} > 0$.

At the time the model was published, it was not appreciated that the role of the force-free magnetic flux rope in the support of the inverse-type prominence sheet is quite general. Once its generality is recognized, we become motivated to do two things. The first is to show that this model is capable of relating several well-known but hitherto disjoint observations. The

second is to introduce cross-field currents in the corona in order to identify the embedding magnetic flux rope with the prominence cavity. The limitation of the force-free flux rope in L93 is obvious. Since this flux rope exerts no force on the corona, it manifests no density structure to correspond to its presence.

Before proceeding, a note about geometry. In the idealized two-dimensional Cartesian geometry used in this paper, the flux rope and the embedded prominence sheet are both infinitely long. In realistic geometry, both these structures are of finite lengths with their ends turned down to the solar surface to blend into the structures at the base of the corona. What the two-dimensional model captures is essentially that these structures in the real corona have a main part of each of their lengths levitating in the corona.

3.2.2. *Prominence-related Active-Region Fibril Patterns*

The standard interpretation seems reasonable that the active-region fibrils observed in Hα delineate the parts in the chromosphere of the magnetic flux tubes extending from the photosphere below (Foukal 1971). We shall adopt this interpretation although exceptions should be born in mind. The fibril-like long prominence or filament is a well-known exception. Given a magnetic-field solution, we can interpret what fibril pattern it will produce in a theoretical chromosphere by the following construction. First trace its lines of force in three-dimensional space up to some given height to correspond to the top of some imagined chromosphere above the plane $z = z_0$ which we have interpreted to be the photosphere. These lines of force when viewed in projection on the plane $z = z_0$ might then correspond to theoretical fibril structures in the imagined chromosphere. In this construction, lines of force anchored to the base $z = z_0$ and oriented close to the vertical will have a smaller part in the imagined chromosphere than those with strong B_x or B_y components.

Figure 7*a* displays the sinistral fibril pattern constructed for the inverse-type prominence magnetic field in Figure 6*c*. Each fibril line is shown with an arrowhead marking its footpoint on $z = z_0$ and indicating the direction of its magnetic field. We recall that the inverse magnetic field in Figure 6*c* is one of a bipolar potential field lying in the y-z plane arching over an arcade of sheared, bipolar magnetic field which, in turn, encases a magnetic flux rope with the embedded prominence sheet. Since the flux rope is fully detached from the base $z = z_0$, its field lines do not show up in Figure 7*a*. What do show up are the lines of force of the two types of anchored fields. Those lines from the sheared field give rise to fibrils with an x-component. Others from the potential field are perpendicular to the polarity-inversion line. As shown in Figure 7*a*, there is a gradual transition of the fibril geometry from one type to the other. On the photosphere $z = z_0$, the flux surface $\partial\sigma$ intersects at the lines $y = \pm (r_0^2 - z_0^2)^{1/2}$. The sheared field is confined within $y^2 < r_0^2 - z_0^2$.

There is qualitative agreement between the theoretical pattern and the observed sinistral pattern sketched in Figure 2, but the correspondence is not impressive. In Figure 7*a*, the theoretical fibrils (1) are longer if they are near the polarity

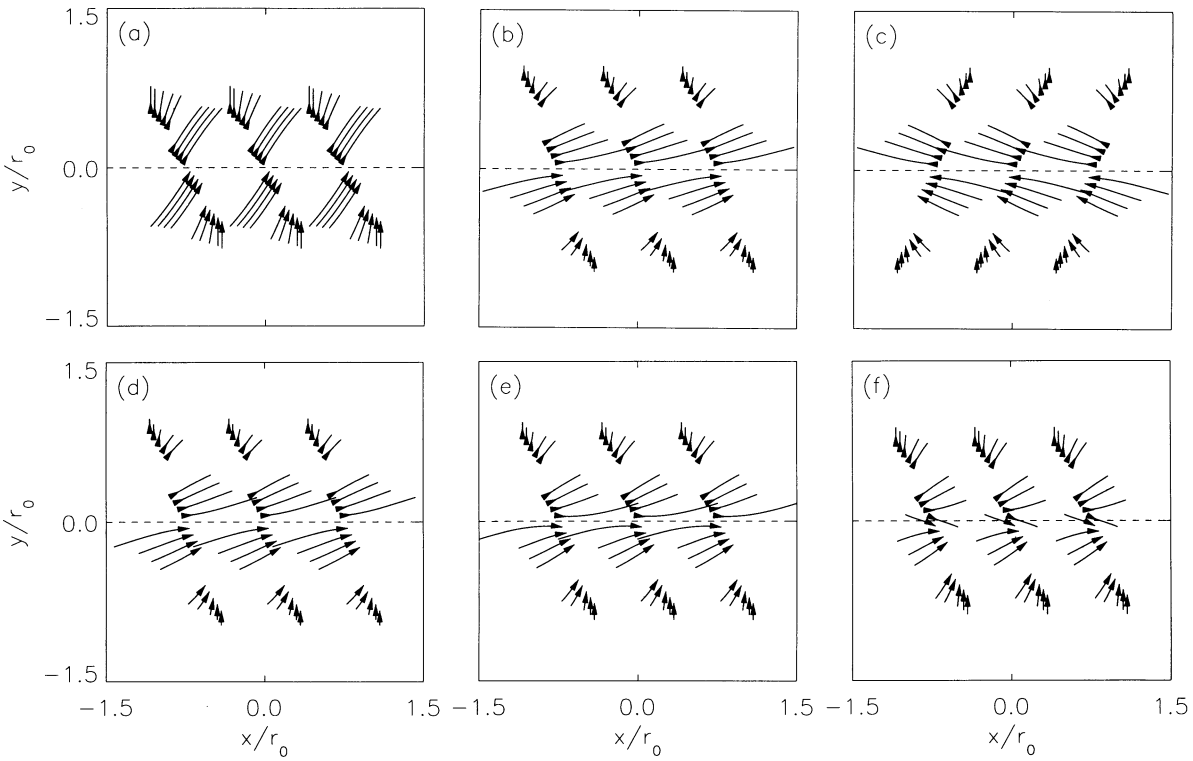

FIG. 7.—Theoretically constructed chromospheric fibrils. Each fibril is represented by a line of force seen projected on the plane $z = z_0$, a constant, representing the photosphere, with an arrow head indicating its footpoint on the photosphere and the direction of the magnetic field. Only the part of the line of force is shown which lies between the photosphere and the chosen height $z = z_0 + 0.2r_0$ representing the top of the artificial chromosphere. The dashed straight line represents the photospheric magnetic-polarity inversion line vertically above which lies the prominence sheet not shown in each case. In all six cases, the region $y > 0$ has positive polarity as indicated by the arrow heads. (*a*) The fibril pattern of the magnetic field shown in Fig. 6*c*; $z_0 = -0.9r_0$. (*b*) The fibril pattern in the dextral configuration of the magnetic field shown in Fig. 8*a*; $z_0 = -0.7r_0$. (*c*) The sinistral counterpart of the fibril pattern in (*b*). (*d*), (*e*), and (*f*) are, respectively, the fibril patterns of the magnetic fields shown in Figs. 11*a*–11*c*.

inversion line, (2) point away from (toward) the inversion line in the positive (negative) polarity region, and (3) do not arc over the polarity inversion lines. These properties are consequences of the presence of the flux rope of twisted magnetic fields. The theoretical fibrils near the inversion lines are parts of the helical lines of force forming the rope. These lines of force, with their main part above the photosphere, thread into the region below the photosphere in a shallow layer to reemerge as they wind along. The only lines of force which thread across the (vertical) z-axis low in the atmosphere belong to the detached flux rope. They do not originate from below the chromosphere. Hence, in the chromosphere which is the low part of the atmosphere, no lines of force emanating from the photosphere arc low over the inversion line. The strong x-component of the winding magnetic field accounts for the long fibrils near the inversion line. Moreover, the x-component of the winding field is stronger the closer the particular field line lies to the axis of the flux rope; that axis lies in $z > z_0$. This implies that the fibrils closer to the inversion lines have greater B_x and are therefore longer; whereas, in the (far) region $y^2 > r_0^2 - z_0^2$, $B_x = 0$ and the fibrils are short and perpendicular to the inversion line. It is interesting to note that the latter are associated with a potential magnetic field which, at the level of the chromosphere, points away from (toward) the inversion line in the magnetically positive (negative) region.

Less impressive is the feature that the theoretical fibrils do not line up well along the inversion line. This arises from the fact that in this solution, the component B_y is relatively strong at the base $z = z_0$.

Another observation also fits well as already pointed out in L93. Repeated observations have revealed that the magnetic field in the prominence sheet tends to increase with height (Rust 1967; House & Smartt 1982; Leroy et al. 1984; Leroy 1989). In Figure 6*c* it is clear that in general for this model, the magnetic field in the y-z plane along the prominence sheet must decrease with height as the O-type neutral point is approached along the sheet (L93). However, the component B_x increases with height as one approaches the O-type neutral point. The latter can dominate so that the net magnetic field increases with height in the prominence sheet. Moreover, the magnetic field vector would align more along the long axis of the prominence as a function of increasing height, such as found in a prominence observed in detail by House & Smartt (1982).

3.2.3. *Filament Channels*

We can bring the theoretical fibril pattern of the model to quite impressive agreement with the pattern in Figure 2 by superposing $A_{\rm shear}$, $A_{\rm prom}$, and $A_{\rm dipole}$. Figure 8*a* shows an example with $\lambda = 4.05$, $a_{\rm prom} = 1.0$, $a_{\rm dipole} = -0.274$, $a_1 = 0$, $a = 0.2$, $b = 0.6$, $z_0 = -0.7$. Again the superposition must ensure that there is sufficient field-aligned current to support the upper part of the inverse-type prominence sheet by attraction from above. This translates into a condition on λ in terms of the other free parameters of the solution; we omit writing it down explicitly. This condition ensures that the net $B_y > 0$ along the prominence sheet so that all lines of force for the given prominence current sheet thread from left to right as shown close up in Figure 8*b*. In this example, the current sheet is relatively weak so that if we remove it from the superposition, the global magnetic field without the prominence sheet looks similar to that shown in Figure 8*a* except that the closed fields sag a little less toward $z = z_0$, and the kink in the magnetic field due to the sheet is gone as shown close up in Figure 8*c*. Comparing Figures 6*c* and 8*a*, we see that we have basically the same global magnetic topology.

The theoretical fibril pattern of this prominence magnetic field in the sinistral configuration is shown in Figure 7*b* and its resemblance to the sketch in Figure 2 is remarkable. In particular, the theoretical fibrils are almost parallel to the inversion

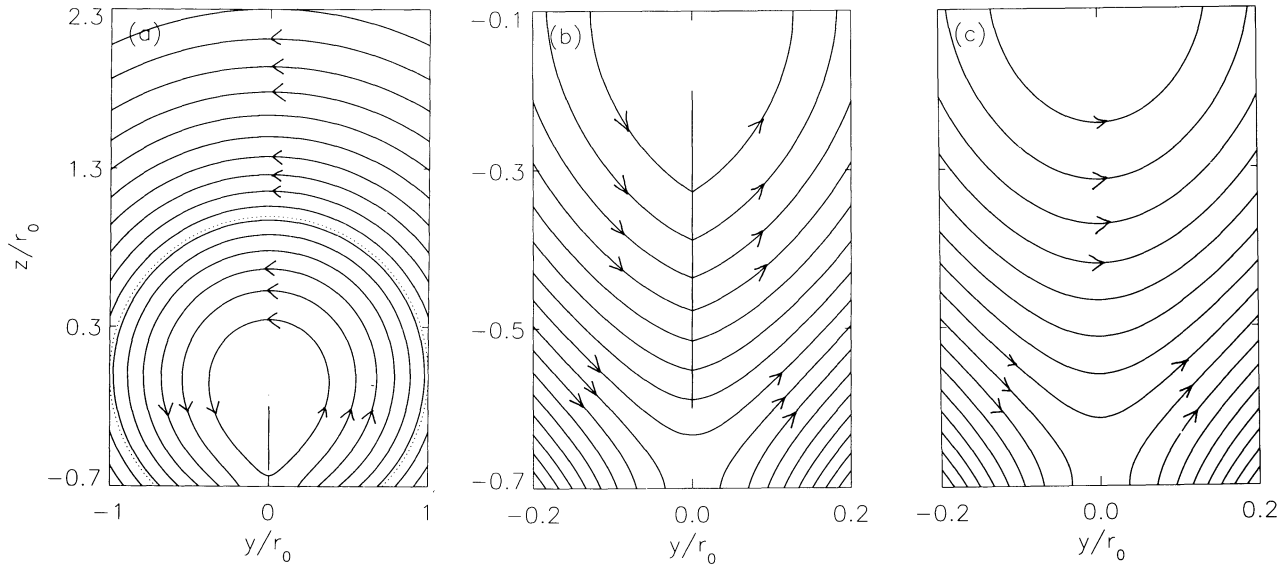

FIG. 8.—The inverse-type prominence sheet embedded in a magnetic flux rope with vanishing B_y and B_z at the inversion line on the photosphere taken at $z = -0.7r_0$. (*a*) The lines of force projected on the y-z plane generated by contours of constant A as a linear sum of $A_{\rm shear}$, $A_{\rm prom}$ and $A_{\rm dipole}$ described in the text. The dotted circle $r = r_0$ centered at the origin is a magnetic flux surface outside of which the field is potential. Within it B_x is not zero due to a force-free electric current density around the prominence sheet represented by the vertical line extending from $z = -0.2r_0$ to $z = -0.6r_0$. The fixed contour interval used gives a tidy density of lines of force but does not show the closed lines of force representing a flux rope which threads the prominence sheet. These lines of force are shown in the close-up view in (*b*) of the prominence sheet. If the term in $A_{\rm prom}$ producing the current sheet in the superposition A is eliminated, the magnetic field has basically the same field projection in (*a*) but a different local field shown close-up in (*c*) without the current sheet.

line on its immediate two sides. This feature is produced by a choice of the coefficients λ, $a_{\rm prom}$, and $a_{\rm dipole}$ such that at the inversion line on $z = z_0$, $B_y = 0$. In the vicinity of this point, the magnetic field is principally in the x-direction, and, hence, the desired fibril pattern is produced.

In the force-balance equation (9), the component $B_x = Q$ appears as the magnetic pressure term Q^2. The mathematical treatment allows Q^2 to take negative values so that solutions with this property need to be rejected on physical grounds. It also means that the constant λ in equation (11) could take either sign without changing the form of A. Take the solution in Figure 8*a* and reverse the sign of λ. This changes the sign of B_x everywhere to produce the fibril pattern in the dextral configuration shown in Figure 7*c*. The fibrils in Figures 7*b* and 7*c* stream in opposite directions although the distributions of the normal field at $z = z_0$ are the same.

The presence of a zone of vanishing B_y in the neighborhood of the inversion line on $z = z_0$ has a separate effect. With the prominence sheet's lower tip located just above the inversion line, B_y would increase with height on the sheet just above the lower tip. This increase, compounded by B_x also increasing with height, would enhance the observed property of the prominence magnetic field being an increasing function of height.

It should become clear from our analysis that the characteristic fibril patterns in Figure 2 do not depend on the presence of the prominence but are intrinsic to the presence of the magnetic flux rope. This is an important physical point. We saw from § 2 that the inverse-type prominence cannot exist without the magnetic flux rope. On the other hand the flux rope without the prominence is a possible equilibrium state; the force-free fields in Figures 6*a* and 8*c* are examples. This theoretical result allows us to understand the observation that the characteristic, streaming-fibril patterns can exist, though not often in the chromosphere independent of the prominence, marking what is commonly referred to as a filament channel (McIntosh 1972; Martin et al. 1993). A prominence is always found within or in a portion of a filament channel, but a filament channel may exist without a prominence. Moreover, it has been suggested that a filament channel can last for several weeks during which more than one filament may form and disrupt in succession (Martin et al. 1993). The streaming of fibrils parallel to the photospheric inversion line is the key feature whether or not the filament is present. We suggest that filament channels correspond to a magnetic flux rope which has made its way from below into the atmosphere above the photosphere, giving rise to these telltale fibril signatures (Low 1994).

A point of interpretation needs to be emphasized so that our model will not be physically misunderstood. Although the solutions we have constructed can be continued mathematically below the level $z = z_0$ (artificially set to be the photosphere), the part of the solution in $z < z_0$ must not be taken seriously in the physical spirit of the model. The solution intended for the region $z > z_0$ must in principle fail to describe the photosphere and below because the physical conditions there are quite distinct and different.

3.2.4. *The Twisted Flux Rope as a Density Cavity*

To model the prominence flux rope as a true density cavity, we need to introduce cross-field currents in the corona. Since the solution $A_{\rm corona}$ has not been treated previously, we first examine its properties separately. Set $\lambda = a_{\rm prom} = a_{\rm dipole} = 0$ so that $A = A_{\rm corona}$, which describes a bipolar magnetic field confined entirely in $\partial\sigma$ by the field-free, polytropic external atmosphere. This magnetic field lies in the y-z plane with $B_x = 0$. Figure 9 shows the lines of force which are circles all tangent to the line $z = -r_0$ at the point $y = 0$, $z = -r_0$. Equations (12) and (13) imply that relative to the external hydrostatic plane-parallel atmosphere, the pressure and density inside $\partial\sigma$ are depleted at the same height. To see this note that if $a_1 > 0$, $A_{\rm corona} < 0$ inside $\partial\sigma$ by equation (20), and that changing the

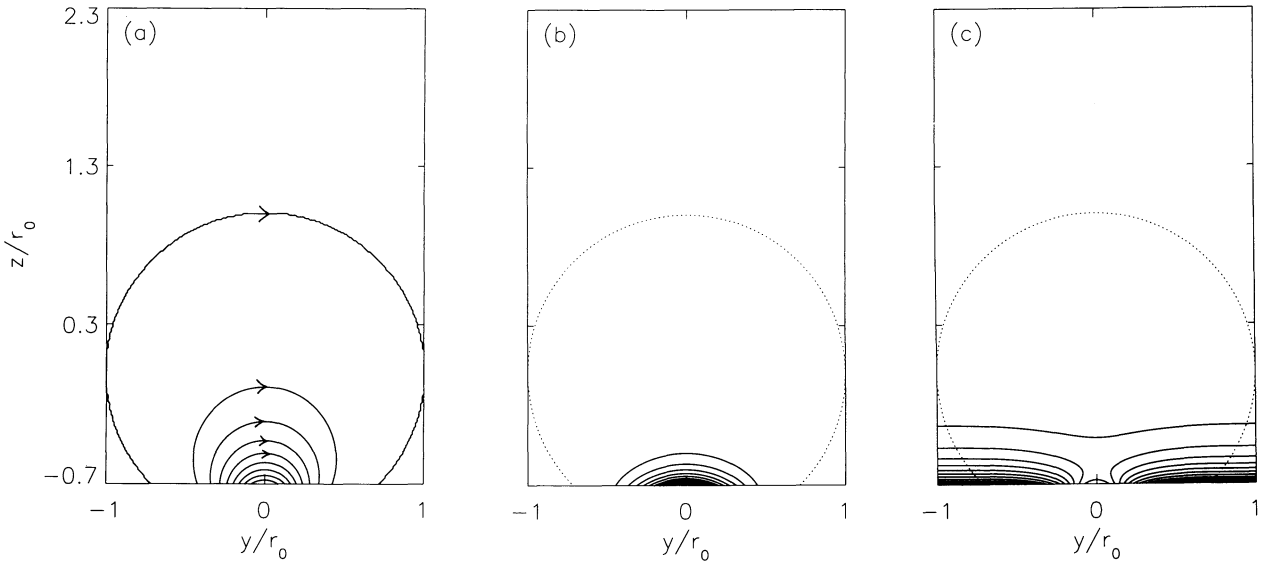

FIG. 9.—The magnetic field generated by $A_{\rm corona}$ associated with pressure-induced, cross-field electric current density. (*a*) The lines of force of constant $A_{\rm corona}$ above the photosphere taken on $z = -0.7r_0$. The last outer line coincides with the circle $r = r_0$ centered at the origin, outside of which the field is identically zero. (*b*) Contours of constant $\Delta\rho$, the difference between the equilibrium density and the plane-parallel hydrostatic density in the exterior of $r = r_0$ obtaining at the same height. By definition $\Delta\rho$ vanishes everywhere outside $r = r_0$, and is negative inside $r = r_0$, with the density deficit increasing in magnitude across the contours of constant change in $\Delta\rho$ in some arbitrarily chosen unit, as shown. The low-density cavity associated with the confinement of the bipolar magnetic field is shown in (*c*) in terms of the contours of constant net equilibrium density. The dotted circle is the magnetic flux surface outside of which the magnetic field is identically zero.

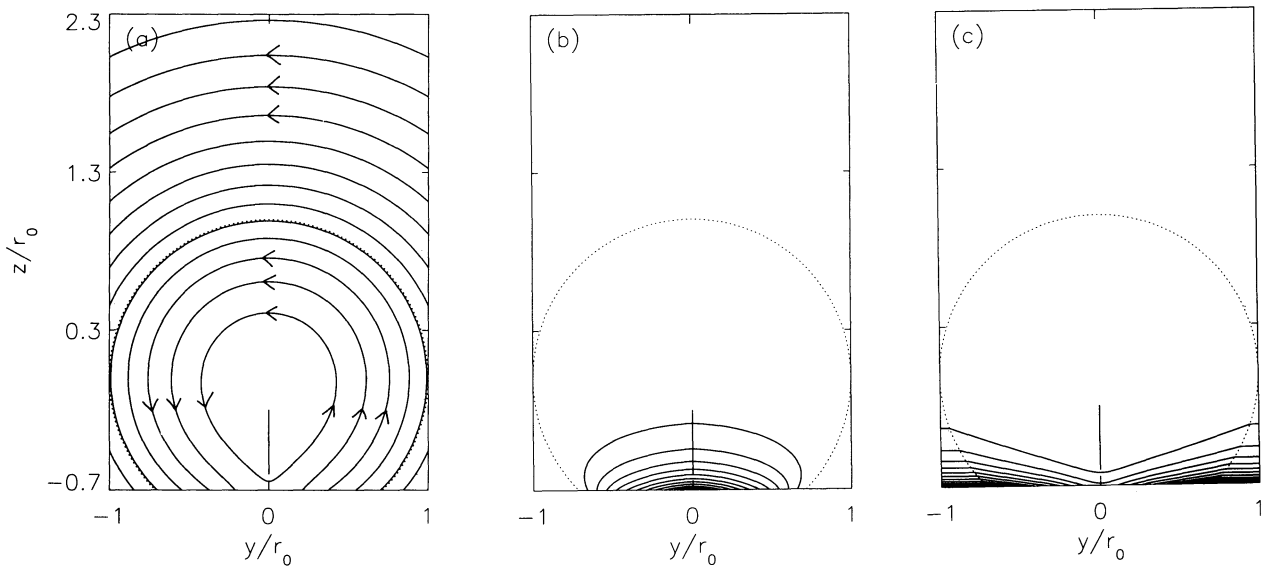

FIG. 10.—The inverse-type prominence sheet embedded in a magnetic flux rope carrying both field-aligned and cross-field electric current densities, with vanishing B_y and B_z at the inversion line on the photosphere taken at $z = -0.7r_0$. (*a*) The lines of force projected on the *y*-*z* plane generated by the contours of constant A as a linear sum of A_{shear}, A_{prom} and A_{corona} described in the text. The dashed circle $r = r_0$ centered at the origin is a magnetic flux surface outside of which the field is potential. Within it, B_x is not zero due to a field-aligned electric current density, and the atmosphere departs significantly from plane-parallel stratification due to the presence of a cross-field current density. Not shown is the magnetic flux rope which threads the prominence sheet represented by the vertical line extending from $z = -0.2r_0$ to $z = -0.6r_0$. These lines of force are shown in Fig. 11*a* in a close-up view. (*b*) The contours of constant density deficit $\Delta\rho$, as defined in Fig. 9, showing the cavity surrounding the prominence sheet represented by the vertical line. (*c*) The prominence and its cavity shown in terms of the contours of constant net equilibrium density.

sign of a_1 would also change the sign of A_{corona}. Hence both pressure and density are independent of the sign of a_1 with $A = A_{\text{corona}}$ in equations (12) and (13). This property does not obtain when A includes a superposition of A_{corona} with the other terms on the right-hand side of equation (16) in the case to be treated below. Figure 9*c* is a plot of constant density showing the depression of density in $\partial\sigma$. If we remove the background density taken to be that given by the plane-parallel density outside $\partial\sigma$, we obtain the deficit $\Delta\rho$ which is everywhere negative inside $\partial\sigma$ and zero outside by definition. It is the weight of the atmosphere which confines the bipolar nonpotential magnetic field inside $\partial\sigma$ in static equilibrium.

We recall that the inverse-type prominence magnetic field in Figure 8*a* is constructed by a linear superposition of A_{shear}, A_{prom}, and A_{dipole}. Let us consider a linear superposition with the potential dipole replaced by the nonpotential dipole A_{corona}. An example is given in Figure 10*a* suspending the prominence sheet as shown in the close-up representation in

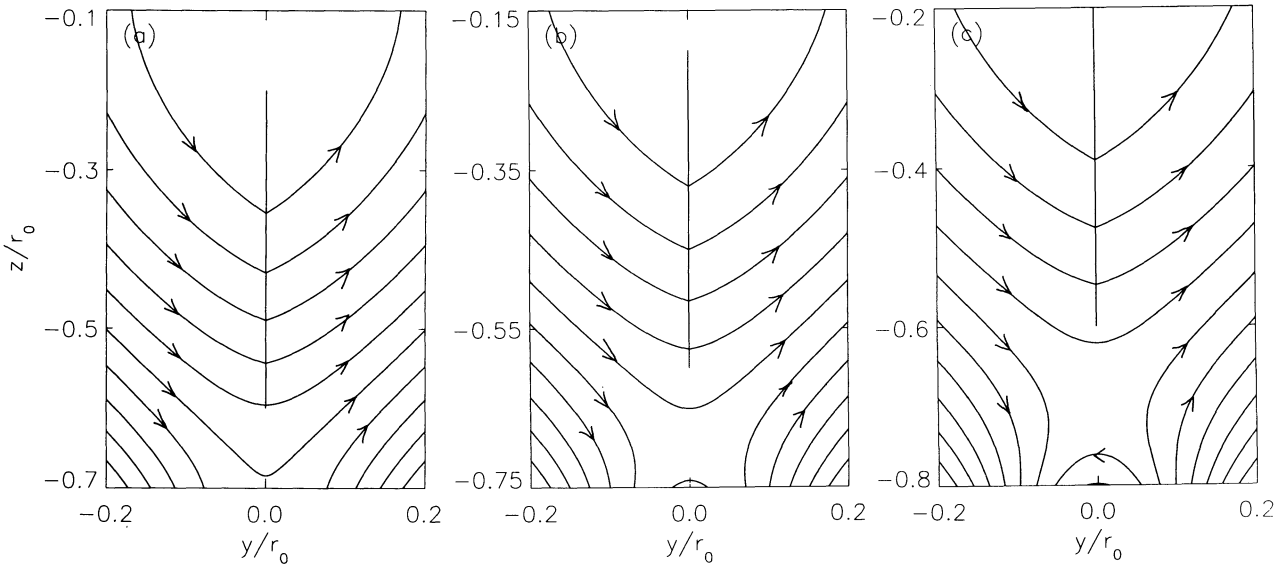

FIG. 11.—Close-up views of the prominence sheet in the magnetostatic solution shown in Fig. 10, with the photosphere taken at $z = z_0$ with (*a*) $z_0 = -0.7r_0$, (*b*) $z_0 = -0.75r_0$, and (*c*) $z_0 = -0.8r_0$, which are the same global field cut at different heights to describe the magnetic field above the photosphere. A gradual transition from zero B_y and B_z at the inversion line on $z = z_0$ to a configuration which has a small amount of flux in $z > z_0$ arching over the inversion line is seen in progression from (*a*) to (*c*).

Figure 11*a*. For this example, $\lambda = 3.51$, $a_{\rm prom} = 1.0$, $a_{\rm dipole} = 0$, $4\pi a_1 = -0.0617$, $a = 0.2$, $b = 0.6$, $z_0 = -0.7$. In this solution, we have again chosen the coefficients λ, $a_{\rm prom}$, and a_1, as given in the caption, such that $B_y = 0$ at the inversion line on $z = z_0$. The fibril pattern produced by this field is shown in Figure 7*d*. The pattern is not different in significant ways from that in Figure 7*b*. However, this new solution admits cross-field currents in the corona around the prominence sheet. The Lorentz force due to this current organizes the corona around the prominence such that this region within $\partial\sigma$ has a density depletion as shown in Figures 10*b* and 10*c*. As noted in the caption, this solution involves a coefficient $a_1 < 0$ so that by equation (12), the coronal density in $\partial\sigma$ is depeleted relative to the exterior density at the same height, since $A > 0$ in that region.

It should be pointed out that suitable superpositions of all four terms on the right side of equation (16) exist to yield a similar inverse-type magnetic field with $a_1 > 0$ and $A > 0$ in $\partial\sigma$. In this case, the region inside $\partial\sigma$ has an enhanced density relative to the exterior and it is the external magnetic field which must play a dominant role to confine the high-pressure plasma as well as the magnetic pressure of the flux rope. In other words, the magnetic flux rope can manifest itself through the cross-field currents both as a high-density region or a low-density cavity. We will take up the significance of this result in the next section. In these constructions, the amplitude a_1 determines the sign of the cross-field current density which generates the Lorentz force around the prominence sheet. Keeping the sign of A in $\partial\sigma$ fixed maintains the bipolar magnetic field in this region to be of one sign. Therefore reversing the sign of a_1 changes the sign of the Lorentz force. In the case of $a_1 < 0$, a cavity is produced in the twisted flux rope. In the opposite case, $a_1 > 0$, a density enhancement is built into the flux rope.

4. DISCUSSION AND CONCLUSION

There are two important results in this paper on the nature of the coronal electric currents in the neighborhood of a quiescent prominence. Let us summarize them and examine some physical implications.

4.1. *Summary of Results*

The first is that prominences in the inverse configuration depend on the presence of volumetric electric currents in the surrounding corona for their support. The mass of a long quiescent prominence is about 10^{15-16} g which is a significant fraction of the total mass of the entire corona (Tandberg-Hanssen 1974). The coronal electric currents required for the support of the prominence may therefore be quite considerable, locally. In order that these currents are substantial and yet not exert an enormous force on the tenuous corona, they must be largely aligned along the local coronal magnetic field. This field-aligned current density naturally gives rise to a flux rope of twisted magnetic fields which embeds the prominence sheet, a configuration which fits observations rather well, in terms of (1) the direction of the prominence magnetic field relative to the field implied by the bipolar magnetic source on the photosphere below, (2) the consistently observed significant magnetic field component along the long axis of the prominence, (3) the general increase of magnetic intensity with height within a prominence, and, (4) the morphology of the chromospheric fibril structures in the neighborhood of an active-region prominence.

The first point has emerged from the first successful static model of the inverse-type prominence configuration presented in L93. However, what was not fully appreciated in L93 is its generality, which we have put on firm theoretical ground in § 2. We now stress a subtle aspect of the theoretical point made in that section. If we do not resolve the prominence as a vertically extended structure (treating it as a line mass, for example) the total weight of the prominence can be balanced by its repulsion by the photosphere, obviating the need to introduce any coronal electric currents around the prominence, as many authors have previously shown (Van Tend & Kuperus 1978; Anzer 1989; Rust 1994). Among the properties characterizing the prominence is its vertical extent. Typically, a prominence is about 5000 km thick and 2–20 times as tall. Even in the limit of neglecting its sheet thickness as a first approximation, the vertical extent of the prominence sheet is an essential property to consider. Then, as shown in § 2, no inverse configuration is possible for the prominence unless coronal currents are present to exert additional forces. To be specific, the coronal currents are required to have the same sign as the prominence current and be located above the prominence. The attraction of the prominence from above by currents of the same sign is needed to counter the self-pinching tendency of the prominence sheet. These effects are suppressed in the oversimplified models, as we now recognize them to be, which treat prominences as a line current. From another physical perspective, we have thus come to appreciate an important electrodynamical implication of a commonly cited property of prominences, namely, their sheet-like structure of great vertical extension.

In the mathematical proof in § 2, we also showed that the other conceptually possible magnetic topology, the normal configuration, is restricted if the corona around the prominence sheet does not contain currents. Only those configurations which contain no closed magnetic fields are admissible, of the type shown in Figure 4*c*. It is interesting that observations of prominence vector magnetic fields suggests that the normal configuration is found only in lower-lying prominences; see the review by Leroy (1989). Moreover, there are even suggestions that they are rare (Martin et al. 1993). For that reason our interest in the normal configuration is minimal. The treatment of the normal configuration in § 2 is included for completeness of the theory.

The coronal currents associated with the flux rope of the prominence in the inverse configuration cannot be everywhere aligned along the magnetic field outside the prominence. To identify the observed low-density cavity around the prominence with the embedding flux rope, we suggest that a component of cross-field current density must be present, even if the field-aligned component is the dominant one. Then the cavity (as well as the high-density helmet dome) can be explained in terms of the Lorentz force generated by the cross-field currents. The demonstration of this point by explicit solutions is the second important result of our paper. This demonstration is not entirely compelling because the model can also admit the flux rope as a region of enhanced plasma. Clearly, to explain the cavity around a prominence we need to look beyond the conditions of force equilibrium to consider the question of mechanical and thermal stability and the evolutionary history of the entire magnetic system. These issues cannot be treated in any degree of completeness without quantitative calculations, and, in any case, they lie outside the scope of this paper. But a tentative, global, physical picture has emerged on these and related issues recently described by Low (1994). To complete our theoretical study here, let us relate what we have learned here to that physical picture.

4.2. *Stability*

Stability is an important factor in the creation of the large-scale helmet structure with its characteristic three-part structure: high-density dome, cavity, and the prominence. Stability analysis of specific magnetostatic equilibria is a nontrivial theoretical undertaking in its own right (Bernstein et al. 1958; Hood 1992; Hu 1988; Low 1990; Zweibel 1981, 1982). We shall give only a heuristic discussion of its role in the formation of the helmet structure. At the minimum, this structure as an ideal magnetohydrodynamic system must be mechanically stable to small perturbations. There are three principal sources of energy for instability: the field-aligned currents, the cross-field currents associated with pressure gradients, and the gravitational stratification (Friedberg 1982). We offer some insights into their roles and interplay.

The flux rope of twisted magnetic fields is susceptible to kink instability associated with the first energy source. On the other hand, unlike the classical force-free twisted magnetic field of the laboratory device, the flux rope in question here is weighted down by the heavy prominence. The kinking of this twisted flux rope therefore involves lifting the prominence in the solar gravitational field. It seems conceivable that the latter may suppress the kink instability during the stable phase of the helmet structure.

The cross-field currents induced by the confinement of pressure by a magnetic field are stabilizing or destabilizing depending on whether the magnetic field is convex or concave, respectively, to the confined plasma. The sharp boundaries, visible in scattered white light, separating the bright (high-density) dome from the external, open-field region and from the cavity, as sketched in Figure 1, bring out very well the issues concerning the stability properties of magnetic curvature. The points labeled 1 and 2 are, respectively, unstable and stable to the interchange mode. In the former, we expect the field strength to increase and the plasma pressure to decrease as we cross the sharp boundary from the high-density dome to the exterior. In the latter, going from the high-density dome into the cavity, the same changes in the two quantities are found except that the magnetic curvature is opposite. The overall stability is, again, complicated by the effect of gravity.

At point 1, the stratification is destabilizing because heavy matter is sitting on light matter just outside of the high-density region. Hence, both magnetic curvature and stratification are destabilizing. We have sketched the outer boundary of the helmet-streamer to have a pronounced bulge near the base to produce the feature of heavy matter over light matter. This was intentionally done to demonstrate the inherent instability of such a configuration. It follows that quiescent helmet-streamers cannot have a bulged geometry at the base, a conclusion we find supportable based on our cursory inspection of recent eclipse photographs.

At point 2, the stratification is destablizing, and it is a competition between the stabilizing magnetic curvature and stratification effects which determines whether stability obtains. For a magnetically dominated plasma under coronal conditions, the magnetic-curvature effect generally is more important, so that the cavity's boundary with the high-density dome is likely to be stable as observed. If this is a valid conclusion, it follows that a high-density flux rope is likely to be unstable, whereas the cavity flux rope in Figure 10 might be stable.

The point labeled 3 in Figure 1 is also interesting. In consequences of the blending of the helmet dome into the long streamer tail, the strong external magnetic field is expected to be convex to the high-density plasma of the helmet-streamer. Moreover, stratification is favorable. So both stratification and magnetic curvature are stabilizing. In this part of the corona, the solar wind is important in the open field region. It follows that the long life of the helmet-streamer must be due to circumstances under which these two stabilizing effects are able to counter the Kelvin-Helmholtz instability (Chandrasekhar 1961) associated with the velocity shear across this interface separating the near static plasma from the solar wind flow.

We have merely pointed out the stability issues and offered some insights into how the various stabilization factors may explain the observed long life of the helmet-streamer. A more quantitative understanding must await proper stability analysis of specific equilibrium states. A quantitative example of the interplay between stratification and magnetic curvature in determining the stability of a magnetostatic structure is given in the Appendix.

4.3. *Origin of Prominences*

Finally, we address the question of the origin of the prominence and its cavity. If we identify the cavity with a magnetic flux rope, we have the result that an inverse-type prominence cannot exist without its cavity; whereas, a cavity without a prominence is a realizable equilibrium state. Moreover, our model suggests that the characteristic chromospheric fibril pattern in the vicinity of an inversion line has a more direct relationship with the twisted flux rope than with the prominence that such a flux rope may embed. These results allow us to understand the well-established observation: The characteristic fibril pattern belongs to a structure called a filament channel which is more fundamental than the prominence in the sense that every prominence is found in a channel, but not all channels need to have a prominence. We propose that the filament channel is the manifestation of the flux rope in the chromosphere.

The global magnetic field containing the prominence is one characterized as a two-flux system: There is the flux system which connects the positive polarity region to the negative polarity region on the two sides of the inversion line; the second flux system is the rope that runs above and parallel to the inversion line. This second flux system may exist in its own right. A magnetic flux rope is an excellent thermal shield, creating an environment in its interior conducive to plasma condensation. This may be the reason for a prominence to be commonly found trapped in a flux rope. From this point of view, the question of origin is more fundamental for the flux rope than it is for the prominence.

The striking resemblance of the theoretical fibril patterns in Figures 7*b*–7*d*, with the observed patterns owes much to the construction which ensures that $B_y = B_z = 0$ at the photospheric inversion line. This construction actually creates an X-type magnetic neutral point at that particular location. Why should such a neutral point arise? The simplest explanation is that a magnetic flux rope has formed below the photosphere and rose into the corona in the scenario proposed in Low (1994). Drainage of matter may result in the breaking of the flux rope into two parallel ones, one to emerge into the corona and the other to sink back down, naturally creating the inverse prominence topology with an X-type neutral point. The neutral point does not have to be located right at the photosphere. Figures 11*b* and 11*c* show examples where the X-type neutral point has risen above the photosphere, giving rise to fibril patterns shown respectively in Figures 7*e* and 7*f*.

Chromospheric observations do not support the pattern in Figure 7*f* for the active-region filaments. The question seems open whether such a pattern might be associated with the quiescent filaments which tend to be located, presumably with their embedding flux ropes, much higher into the corona. The dynamical, buoyant rise of a magnetic flux rope in a stratified medium merits further theoretical study in the above physical context (Parker 1955, 1979; Matsumoto et al. 1993; Shibata et al. 1990).

Over the years, Hα observations of magnetic flux emergence have suggested that the magnetic field emerged highly twisted (e.g., Kurokawa 1987; Tanaka 1991; Wang & Tang 1993). Whereas previous interpretations tend to view these magnetic fields to remain, after emergence, as simple bipolar lines of force with the two feet anchored in the photosphere, the fibril patterns of filament channels suggest that a main part of the rising flux rope may be bodily lifted into the low corona. More recent observations have suggested that magnetic flux systems may, indeed, emerge as essentially detached systems to produce a closed magnetic field connected only to a shallow layer below the photosphere (Lites et al. 1994). It is also possible that the flux rope loses its geometric integrity as it emerges through the photosphere since at this level and below, the plasma pressure and kinetic motion dominate. Given the astronomical scales of these magnetic fields, the net magnetic helicity of the system cannot change over the typical magnetohydrodynamic time-scales of the evolution (Berger 1984). Thereore, if the emerging magnetic field has a net magnetic helicity despite its turbulent, tangled state, it will relax to a large-scale, organized flux rope upon entering the tenuous corona carrying that conserved endowed net helicity (Low 1994). This relaxation proceeds via rapid reconnection of the magnetic field. Presumably this is the flaring that accompanies flux emergence (e.g., Wang & Tang 1993). When the magnetic flux rope has formed following the destruction of small-scale structures, the magnetic isolation of the plasma on the rope naturally promotes plasma condensation. Consequently the prominence forms, the flux rope becomes a density cavity, and the structure attains stability for a spell (Athay, Jones, & & Zirin 1985a, b).

As to how the peculiar two-flux system of the prominence might be possible above a locally bipolar region on the photosphere, we need to leave our two-dimensional Cartesian model to a fully three-dimensional model. In the two-dimensional model, the second flux system is an endless or infinite flux rope which is wholly levitated in the atmosphere taken as an infinite plane. What this model has captured of the realistic situation is the aspect of a flux rope with a principal length of it suspended in the atmosphere above the photosphere. The end topology of the flux rope is approximated out of the idealized two-dimensional model. We refer to Lites et al. (1994) for a three-dimensional model of a two-flux magnetic system topologically quite compatible with a photospheric bipolar region of finite spatial extent, such as observed of real prominences.

The reality of the inverse magnetic configuration, the increase of the prominence magnetic field with height, the fibril patterns of filament channels, are disjoint observations which have been with us for more than 10 years. These and other pieces of observations, including recent vector field measurements, begin to relate and to make physical sense as a whole through the simple models presented in this paper. It appears that we are beginning to understand the magnetic topology of prominences. In addition to the quantitative results in §§ 2 and 3, which form the basis of our analysis, we also derived several implications and raised some questions for further work. If these implications are in the correct physical direction, we may also have gotten a glimpse of the origin of prominences and their role in solar activity (Low 1994).

This work was initiated during the sabbatical visit of J. R. H. to the High Altitude Observatory. We thank Dick White for helpful comments, and the anonymous referee for pointing out an important reference.

APPENDIX

A NONLINEAR MAGNETOSTATIC SOLUTION AND ITS STABILITY

If there is no current sheet and no field-aligned currents, equation (9) reduces to

$$\nabla^2 A + 4\pi \frac{\partial p(A, z)}{\partial A} = 0 . \tag{A1}$$

The prescription involving an arbitrary functional form $P_0(A)$:

$$p = \frac{P_0(A)}{(z + r_0)^2} , \tag{A2}$$

$$\rho = \frac{2P_0(A)}{g(z + r_0)^3} , \tag{A3}$$

gives a plasma distribution which satisfies the hydrostatic equilibrium equation (8) along the magnetic lines of force. The magnetostatic problem then reduces to solving for A in equation (A1) which now takes the form

$$\nabla^2 A + \frac{4\pi}{(z + r_0)^2} \frac{dP_0(A)}{dA} = 0 . \tag{A4}$$

A particular class of solutions of this nonlinear equation can be obtained by taking A to be a strict function of ζ defined by equation

(21). Then equation (A1) can be brought to the following quadrature:

$$4\pi a_1 P_0(A) + \frac{1}{2}\zeta^2\left(\frac{dA}{d\zeta}\right)^2 - \int^{\zeta} \zeta\left(\frac{dA}{d\zeta}\right)^2 d\zeta = 0 . \tag{A5}$$

This remarkable result shows that the $n = 2$ polytropic atmosphere admits an infinity of magnetostatic solutions in which the magnetic lines of force are in the form of the family of circles generated by constant values of ζ, all touching the line $z = -r_0$ at $y = 0$, $z = -r_0$. Among the many solutions is the special case $A = A_{\rm corona}$ with $P_0 = a_1 A + a_0$ given in § 3. The magnetic field is given by

$$\boldsymbol{B} = \frac{dA}{d\zeta}\nabla\zeta . \tag{A6}$$

We are quite free to prescribe the distribution of the magnetic intensity through the free function $dA/d\zeta$. The result is in general a nonpotential field whose Lorentz force is balanced in equilibrium by a distribution of plasma described by equations (A2) and (A3), where $P_0(A)$ is the pressure profile, related to the prescribed $dA/d\zeta$ by equation (A5). In particular, the prescription of $A = \zeta$ gives the well-known potential dipole magnetic field for which P_0 is uniform in space and equations (A2) and (A3) describe a self-supporting hydrostatic atmosphere.

The construction is analogous to the classical situation of a static magnetic field in the form of parallel straight lines of force in balance against pressure gradients, in the absence of gravity. In this case, one could prescribe an arbitrary distribution of magnetic intensity on the straight lines of force and maintain equilibrium with a pressure distribution which renders the sum of magnetic and plasma pressures uniform in space.

The magnetic field (A6) is (in general) nonpotential but has exactly the same field-line geometry as the potential field due to a point dipole. The two fields have different distributions of magnetic intensity over the same lines of force. Hu (1988) has given a powerful sufficient condition for the stability of this type of nonpotential field as a magnetostatic equilibrium state. The condition deals with the gradients of the magnetic pressures of the nonpotential magnetic field and its associated potential field, across their common set of lines of force. Take the gradients in the direction of decreasing magnetic pressure for the potential field. Then, the equilibrium with the nonpotential field is stable if the gradient of the magnetic pressure is everywhere steeper than that of the corresponding gradient for the potential field.

The steeper magnetic-pressure gradient described above would correspond to an equilibrium in which a locally enhanced magnetic field is confined by a surrounding region of high-pressure plasma. For the magnetic field (A6), this situation is one where a low-density, strong bipolar magnetic field is confined by an external low-field, high-density plasma. By Hu's condition such an equilibrium state is stable. The stability derives from the favorable magnetic curvature force dominating over the destabilizing density stratification involving the external heavy plasma sitting on top of the magnetic cavity. The static equilibrium shown in Figure 9 is an explicit example of this type of stable states. By the same condition, an equilibrium constructed from equation (A6) for a localized, high-density, lower field region confined by an external, field-dominated, low-density region may be unstable. In this case, the magnetic curvature is unfavorable and may dominate over the stabilizing density stratification.

REFERENCES

Amari, T. 1990, in Advances in Solar System Magnetohydrodynamics, ed. E. R. Priest (Dordrecht: Reidel), 3
Amari, T., & Aly, J. J. 1990, A&A, 231, 213
Anzer, U. 1989, in Dynamics and Structure of Quiescent Solar Prominences, ed. E. R. Priest (Dordrecht: Kluwer), 143
Athay, R. G., Jones, H. P., & Zirin, H. 1985a, ApJ, 288, 363
———. 1985b, ApJ, 291, 344
Athay, R. G., Querfeld, C. W., Smartt, R. N., Landi degl'Innocenti, E., & Bommier, V. 1983, Sol. Phys., 89, 3
Berger, M. A. 1984, Geophys. Astrophys. Fluid Dyn., 30, 79
Bernstein, I. B., Frieman, E. A., Kruskal, M. D., & Kulsrud, R. M. 1958, Proc. R. Soc. Lon., A244, 17
Cartedge, N., & Hood, A. W. 1993, Sol. Phys., 148, 253
Chandrasekhar, S. 1961, Hydrodynamic Stability (Oxford: Oxford Univ. Press)
Coulson, C. A. 1958, Electricity (Edinburgh: Oliver and Boyd)
Demoulin, P., & Forbes, T. G. 1992, ApJ, 387, 394
Drago, F. C., & Felli, M. 1970, Sol. Phys., 14, 171
Foukal, P. 1971, Sol. Phys., 19, 59
Friedberg, J. P. 1982, Rev. Mod. Phys., 54, 801
Hagyard, M. J., & Rabin, D. M. 1986, Adv. Space Res., 6, 389
Hood, A. W. 1992, Plasma Phys. Contr. Fusion, 34, 411
House, L. L., & Berger, M. A. 1987, ApJ, 323, 406
House, L. L., & Smartt, R. N. 1982, Sol. Phys., 80, 53
Howard, R. 1972, Sol. Phys., 25, 5
Hu, Y. Q. 1988, ApJ, 331, 402
Hundhausen, A. J. 1977, Coronal Holes and High Speed Wind Streams, ed. J. B. Zirker (Boulder: Colorado Assoc. Univ. Press)
———. 1994, in The Many Faces of the Sun, ed. K. Strong, J. Saba, & B. Haisch (New York: Springer), in press
Hundhausen, J. R., & Low, B. C. 1994, ApJ, 429, 876 (Paper I)
Illing, R. M. E., & Hundhausen, A. J. 1986, J. Geophys. Res., 91, 10, 951
Jackson, W. D. 1965, Classical Electrodynamics (New York: Wiley)
Kahler, S. 1987, Rev. Geophys., 25, 663
Kundu, M. R., Melozzi, M., & Shevgaonkar, R. K. 1986, A&A, 167, 166
Kurokawa, H. 1987, Sol. Phys., 113, 259
Leroy, J. L. 1989, in Dynamics and Structures of Quiescent Solar Prominences, ed. E. R. Priest (Dordrecht: Kluwer), 77
Leroy, J. L., Bommier, V., & Sahal-Brechot, S. 1984, A&A, 131, 33
Lites, B. W., Low, B. C., Martinez Pillet, V., Seagraves, P., Skumanich, A., Frank, Z. A., Shine, R. A., & Tsuneta, S. 1994, ApJ, in press
Low, B. C. 1990, ARA&A, 28, 491
———. 1993, ApJ, 409, 798, L93
———. 1994, Phys. Plasmas, 1, 1684
MacQueen, R. M. 1980, Phil. Trans. R. Soc. Lon., A297, 605
Martin, S. F., Bilimoria, R., & Tracadas, P. W. 1993, in Solar Surface Magnetism, ed. R. J. Rutten & C. J. Shrijver (Dordrecht: Kluwer), 303
Matsumoto, R., Tajima, T., Shibata, K., & Kaisig, M. 1993, ApJ, 414, 357
McIntosh, P. S. 1972, Progr. Astronault. Aeronault., 30, 65
Newkirk, G., Jr. 1967, ARA&A, 5, 213
Parker, E. N. 1955, ApJ, 121, 491
———. 1979, Cosmological Magnetic Fields (Oxford: Oxford Univ. Press)
Pneuman, G. W., & Kopp, R. A. 1971, Sol. Phys., 18, 258
Priest, E., ed. 1989, Dynamics and Structure of Quiescent Solar Prominences (Dordrecht: Kluwer)
Ridgway, C., Amari, T., & Priest, E. R. 1991a, ApJ, 367, 321
———. 1991b, ApJ, 378, 773
Rust, D. M. 1967, ApJ, 150, 313
———. 1994, On the Direction of Magnetic Fields in Filaments, preprint
Saito, K., & Hyder, C. L. 1968, Sol. Phys., 5, 61
Saito, K., & Tandberg-Hanssen, E. 1973, Sol. Phys., 31, 105
Shibata, K., Nozawa, S., Matsumoto, R., Sterline, A. C., & Tajima, T. 1990, ApJ, 351, L25
Sime, D. G., & Streete, J. 1993, ApJ, 408, 368

Straka, R. M., Papagiannis, M. D., & Kogut, J. A. 1975, Sol. Phys., 45, 131
Sturrock, P. A., & Smith, S. M. 1968, Sol. Phys., 5, 87
Tanaka, K. 1991, Sol. Phys., 136, 133
Tandberg-Hanssen, E. 1974, Solar Prominences (Dordrecht: Reidel)
Van Tend, W., & Kuperus, M. 1978, Sol. Phys., 59, 115
Vrsnak, B., Ruzdjak, V., & Rompolt, B. 1991, Sol. Phys., 136, 151
Wang, H., & Tang, F. 1993, ApJ, 407, L89
Wu, F., & Low, B. C. 1987, ApJ, 312, 431
Zirin, H. 1988, Astrophysics of the Sun (Cambridge: Cambridge Univ. Press)
Zweibel, E. G. 1981, ApJ, 249, 731
———. 1982, ApJ, 258, L53